LASER INDUCED DAMAGE IN LITHIUM FLUORIDE SINGLE CRYSTALS

BY

NAOUFEL SOUGUIR

A THESIS

Submitted to
Michigan State University
in partial fulfillment of the requirements
for the degree of

MASTER OF SCIENCE

Department of Metallurgy, Mechanics
and Materials Science

1990

ABSTRACT

LASER INDUCED DAMAGE IN LITHIUM FLUORIDE SINGLE CRYSTALS

BY

NAOUFEL SOUGUIR

A CO_2 laser with radiation wavelength λ=10.6μm was used to laser-irradiate lithium fluoride single crystals on their (001) faces. The effects of changing the laser power, the laser pulse length, the distance from the laser focus to the sample surface, and the sample thickness were investigated. The samples were then etched using a dilute solution of ferric chloride in order to reveal the slip distribution induced by thermal stresses.

Optical and scanning electron microscopy were used to reveal the laser-induced damage on the surface and inside the bulk. The results proved the existence of a laser-induced damaged zone (D.Z) on the surface. This zone included areas of (1) plastic deformation, (2) melting, and (3) vaporization. A ripple pattern in the shape of a helix was observed inside the molten zone. Primary and secondary cleavage cracks were also observed. The length of each type of cleavage cracks depended mainly on the energy density of the treatment. The size and the distribution of the damage was found to be dependent on the extent of the different laser variables and the sample thickness.

The slip distributions inside and outside the D.Z were different due to the different directions of the thermal stresses.

I dedicate this thesis to my mother whose sacrifices I will always remember.

ACKNOWLEDGEMENTS

I would like to thank my adviser Professor K. N. Subramanian for his substantial help and advice throughout the project. I would also like to thank Dr P. Khan and M. Cherif for their assistance on the CO_2 Laser.

I would also like to express my gratitude to R. Vaidya for his great assisstance in using the equipments I needed for this project.

Finally, I'm grateful to Professors K. Mukherjee and E. Case for their valuable suggestions towards the end of this project.

TABLE OF CONTENTS

LIST OF TABLES

PAGE

LIST OF FIGURES

PAGE

INTRODUCTION

Lasers, discovered two decades ago are used extensively in today's technology particularly in metallurgy and materials science. A laser is a device that uses the principle of amplification of electromagnetic waves by stimulated emission of radiation and operates in infrared, visible or the ultraviolet region.

Laser output is powerful because atoms can be stimulated to emit electromagnetic radiation much faster than they would spontaneously. The laser output consists of a nearly monochromatic, high-intensity, coherent wave [1]. Coherent light has a single frequency or one color [2].

Pulse-lasers generate high power (the shorter the pulse is, the higher the output power of the laser) with plane wave radiation. The focused beam from pulsed lasers can generate energy densities at which all materials melt and vaporise. It is possible to drill holes or to weld materials with a laser beam, the precision being very high [3].

An electromagnetic wave in contact with a solid material could be reflected, scattered, absorbed, transmitted or a combination of these phenomena, depending on the material's structure and its electrical properties.

Different materials absorb electromagnetic radiations in different ranges of wavelengths and are said to have

different absorption bands. Absorption refers to the decrease of intensity of electromagnetic waves as it passes through a substance [4], and is represented by an absorption coefficient (α) which depends on the wavelength of the incident wave interacting with the material. Scattering also contributes to the decrease of intensity of waves transmitted through a material. Therefore (α) for a general case can be written as:

$$\alpha = \alpha_a + \alpha_s,$$

where (α_a) is due to true absorption and (α_s) is due to scattering.

Absorption bands also depend on the electrical conductivity of the solid or liquid. Good electrical conductors like metals exhibit general absorption with a minor dependence on wavelength in most cases; but dielectric materials which are poor electric conductors have selective absorption and are said to have absorption bands. However, one material could have more than one absorption band in a spectral region [4].

There is however a relation between reflection and absorption; so high reflection of light usually means high absorption and both have the same wavelength bands [4].

Many ceramic materials allow penetration of electromagnetic radiation without appreciable attenuation. The velocity (v) of propagation of a wave is reduced slightly by the losses in the medium; it is defined as [5]:

$$v \approx 1/\sqrt{\epsilon\mu}$$

where ϵ is the dielectric constant and μ is the permeability of the medium. Such substances must be electrical nonconductors since conduction is related to the appearance of Joule heat [6,7]. This is an irreversible phenomena in which the electromagnetic energy is destroyed or more precisely transformed into heat and in consequence an electromagnetic wave in a conductor is attenuated. In metals, unlike in many ceramic materials, the electrical conductivity is very high and the effect described above is so large that they are practically opaque [8].

Scattered light from the surface can arise from various sources: (1) Defects, whose dimensions are large compared to the wavelength of light. (2) Isolated defects in which dimensions are comparable with the wavelength of light. (3) Micro-irregularities in which heights are small compared to the wavelength of light; these produce scattering.

The prevalent source of scattering from the surface are the micro-irregularities because all surfaces have them from the finishing process. These micro-irregularities are distributed over the entire surface and hence contribute a larger fraction of the scattering, particularly in the visible and ultraviolet, than do isolated surface defects such as scratches, digs, and dust particles.

For smooth but wavy surfaces the scattered light is maximum at about the specular direction (normal to the

surface); rougher or matte surfaces scatter the light more equally in all directions. Surface irregularity is specified in terms of the rms roughness. The rms roughness (δ) of a surface is the root-mean square of the heights of irregularities on the surface. Its unit is usually (Å). The rms roughness determines the total integrated scattering [9].

The fraction of the electromagnetic energy that is not scattered, reflected or transmitted is absorbed by the material and causes its thermal energy to rise.

In general, thermal energy in a solid is aquired by:

1) Vibrational energy, by which atoms vibrate around their lattice positions with an amplitude and frequency that depend on the temperature until the Debye temperature is exceeded; then they vibrate at a relatively constant frequency, called the Debye frequency. This vibration of the atoms around their equilibrium positions (or lattice vibrations) increases the energy of the crystal. One can consider the vibrational spectrum in terms of excitation of phonons. When (p) phonons in a given lattice are excited, the additional energy of the crystal is (phw), where (h) is plank's constant and (w) is the phonon frequency[10].
2) Rotational energy for crystals having rotational degrees of freedom.

3) The energy level of electrons.

4) Changing atomic positions by forming vacancies, interstitials, magnetic orientation or altering the structure of glasses at the transformation range [11].

For ceramic materials, at low temperatures, the lattice vibrations or phonon conductivity is the major factor for the transportation of thermal energy. However, at higher temperatures, the formation of vacancies, interstitials, magnetic disorder and electronic effects contribute to the transportation of heat. The contribution from such defects depends mainly on the structure.

Thermal Properties of Ceramics

Heat capacity and thermal conductivity determine the rate of temperature change in a ceramic. They are fundamental in approximating the resistance to thermal stresses.

1. Heat Capacity

Heat capacity measures the energy required to raise the temperature of a material and is either defined at constant pressure or constant volume. C_p and C_v, the heat capacity at constant pressure and volume respectively are given by:

$$C_p = (dQ/dT)_p = (dH/dT)_p \quad \text{in cal/mole } ^oC, \quad (1)$$

$$C_v = (dQ/dT)_v = (dU/dT)_v \quad \text{in cal/mole } ^oC, \quad (2),$$

and

$$C_p - C_v = \alpha^2 V_o T/\beta \quad (3)$$

where (Q) is the heat exchanged, (U) is the internal energy, (H) is the enthalpy, α=dv/vdT is the volume thermal expansion coefficient, β=-dv/vdp is the compressibility, v is the volume, and V_o is the molar volume. At temperatures above a few hundred degrees centigrade, the heat capacity varies very slowly and linearly with temperature.

2. Heat conduction

For heat conduction the determining equation is:

$$dQ/dt = KA \text{ grad } T \qquad (4)$$

The amount of heat flowing normal to the area (A) in time (dt) is (dQ). The temperature gradient (grad T) measures the change in temperature as a function of position and (K) is the thermal conductivity [11].

Thermal Stresses Due to Rapid Heating on The Surface.

High local thermal expansion can be due to rapid heating at the surface. The rapid heating can be provided by lasers. The sudden rise of the surface temperature to values far above that of the surrounding material results in relaxation of compressive surface stresses. Subsequent rapid cooling of the surface by self-quenching results in tensile stresses and can cause the formation and propagation of cracks [12].

Self-quenching is a mechanism that occurs if sufficient laser power is available (generally more than 7.5 kw), so

that the surface heating is very rapid and the core remains cool. The cold core then quenches the heated surface [13]. Typical quench rates in metals are of the order of $10^{6o}Csec^{-1}$ although the use of Q-switched lasers has recently extended the quench rates to the $10^{10}\ ^{o}Csec^{-1}$ range [14].

Highly localized thermal expansion due to a rapid heating pulse at the surface causes a stress wave to propagate into the interior of the solid. The magnitude of the peak stress depends on the laser pulse duration. Cracking and fracture could occur even in a very ductile metal with a laser pulse lasting few nanoseconds [15].

The formation of high thermal stresses during laser processing is not desirable because it can cause micro-cracking and a decay in the strength of the material. The strength retained after shocking depends on the length of the cracks present within the shocked material [16].

High-intensity laser beams ($10^{9}watts/cm^{2}$) pulsed on the surface induce pressures on the surface. The pressures propagate into the bulk as high amplitude stress waves. Microstuctural examination of the laser-shocked surface shows a plastically deformed metal with a high dislocation density and residual stess. An increase in the hardness and strength are also registered [17].

Merkle and Bass measured the multiple pulse laser-induced bulk damage in crystalline and fused quartz at wavelengths of 1.064 and 0.532 micrometer [18]. They

reported that the single pulse damage threshold varied insignificantly among materials or with wavelength. The multipulse induced damage depended strongly upon the material and the laser wavelength. The number of pulses needed to produce macroscopic damage as a function of intensity is indicative of an accumulation process in which some minimum intensity is required to initiate the accumulation of microscopic damage which leads to macroscopic damage.

Musual [19] analysed the stress-strain behavior of the near surface region of laser treated copper mirrors. They suggested that the elastic response is maintained below a certain surface temperature rise (δT_y), which depends on the yield stress, modulus of elasticity, poisson's ratio, and the coefficient of thermal expansion of the metal. The value of δT_y was determined to be:

$$\delta T_y \approx (1-\mu)Y/E\alpha \qquad (5)$$

where (μ) is poisson's ratio, (Y) is the yield stress, (E) is Young's modulus, and (α) is the coefficient of thermal expansion [19,20,21].

For a temperature rise δT above δT_y, plastic strain accumulates after the first single laser pulse. Musual developed a model to show that plastic strain accumulates during each successive laser pulse and is proportional to the temperature rise above $2\delta T_y$. This plastic strain induces the formation of slip bands and intergranular slip

at the surface [19]. The slip lines are produced along favorable crystallographic orientations [21]. These crystallographic orientations have maximum resolved shear stress and are inclined at 45 degrees with respect to the direction of applied stress [19,23].

Musual also developed an expression for the pulse fluence threshold (F_y) for first-pulse plastic yield. F_y is a function of the optical absorptance, pulse fluence, pulse duration, thermal conductivity, density, and specific heat. The threshold for multipulse accumulation of plastic deformation is $2F_y$.

Musual explained the thermomechanical stress induced by lasers on the surface of a metal. He suggested that as a result of the very rapid temperature rise on the surface, the metal tends to expand but is stopped by "inertial forces" or stesses. The stresses are relieved very fast in the direction normal to the free surface due to outward displacement of the surface. However, strains in directions parallel to the free surface are blocked by the surrounding material. This can induce very large compressive stresses in these directions. When the temperature rise and the coefficient of thermal expansion reach a high enough level, the compressive stresses can exceed the elastic limit of the metlal. The metal is then plastically deformed in compression. The compressive plastic strain, in return, induces tensile stresses that occur during cooling. The

tensile stresses can induce tensile plastic strain. Thus compressive and tensile plastic strains can accumulate during multipulse laser irradiation of a ductile material [19,21].

When the laser fluence exceeds the threshold for plastic deformation by a large amount, ripple patterns, melting, and boiling can occur in copper and aluminum as described by Yong Jee et.al [21]. They also noted that during multipulse operation, planes more favorable for slip can accumulate larger plastic strain than planes that are energetically less favorable [21].

Haessner and Seitz [22] indicated that mechanical stress fields of nearly radial symmetry are induced by laser-heating of (111) surfaces in copper single crystals [22,25]. Figure.1 is a schematic comparing the laser-generated and explosively generated stress waves in a solid [25]. Slip systems were found to be operative only if the radial stresses are high enough. The components of the stress near the surface regions were found to be:

$$\sigma_{rr} = -(1/2)E\alpha\delta T(R/r)^2 \quad \text{for } r>R \ , \qquad (6)$$

$$\sigma_{\phi\phi} = +(1/2)E\alpha\delta T(R/r)^2 \quad \text{for } r>R \ , \text{ and} \qquad (7)$$

$$\sigma_{rz} = \sigma_{zz} = 0 \qquad (8)$$

where r,ϕ,z are the cylindrical coordinates and (R) is the radius of the heat affected zone [22]. (δT) is the temperature increase on the surface due to the laser heating[22].

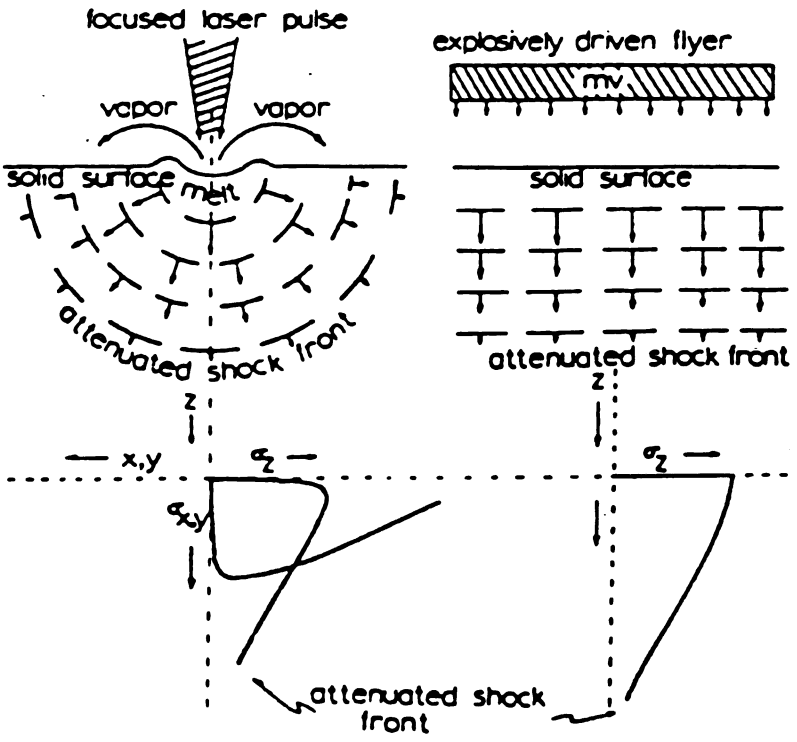

Figure.1 Schematic Comparison of Laser Generated and Explosively Generated shock waves in a solid, from [25].

Porteus et al. [23] noted that at very high temperatures, when melting and evaporation occur, compressive stress can be produced by a reaction pressure on the target due to ejection of vapor [23,24]. Evaporative or plasma-induced compression on the crater and surrounding area results mainly in a normal stress while compression due to thermal expansion at lower fluences is mostly parallel to the surface [23]. Measurements for vapor particle emission in copper and aluminum indicate that plasma-induced compression is actually considerable at very high laser fluences [23].

McMordie et al. [26] showed that although plasma reflectivity was low, a very thin layer of plasma on the surface of the target under high enough laser fluences can greatly attenuate the incoming laser beam which eventually would lose contact with the surface. Following this effect, radial stresses due to thermal expansion are not active anymore and the main form of stress acting on the surface at very high laser fluences is the plasma-induced compression normal to it [24,26].

The purpose of this research is to observe the laser-induced damage in Lithium Fluoride single crystals. Lithium Fluoride has many advantages that help assess the laser-induced damage on the surface or inside the bulk [27].
1) Transparency. This permits the damage to be easily seen and characterized by transmitted light and with low

magnification optical microscopy.

2) The crystals can be easily cleaved for specimen preparation. This also facilitates the study of internal damage. Laser irradiated specimens can be cleaved to check the damage in the cross-sectioned view.

3) The simple well defined slip systems [28,29].

Lithium Fluoride is an ionic crystal and has NaCl structure as illustrated in Figure.2. The primary slip system is {110}<110>. The secondary slip system is {001}<110>. The schematic showing the six {110} planes projected onto the (001) plane is given in Figure.3 [30]. The six solid lines in the Figure represent the traces of the six planes. The four traces in the <100> directions correspond to slip planes that lie at 45 degrees to the surface. They are called the 45 degree slip planes. The two diagonals in the figure are the traces of the planes that lie at 90 degrees to the surface. They are called the 90 degree slip planes.

Fracture Behavior of Lithium Fluoride.

Lithium Fluoride is a semi-brittle material. It exhibits both elastic and limited plastic behavior [29]. Moderate plasticity exists in LiF at room temperature. At high temperatures LiF and most NaCl crystal structured crystals are considered ductile with five independent slip systems within the slip systems {110}<110>, {001}<110>, and

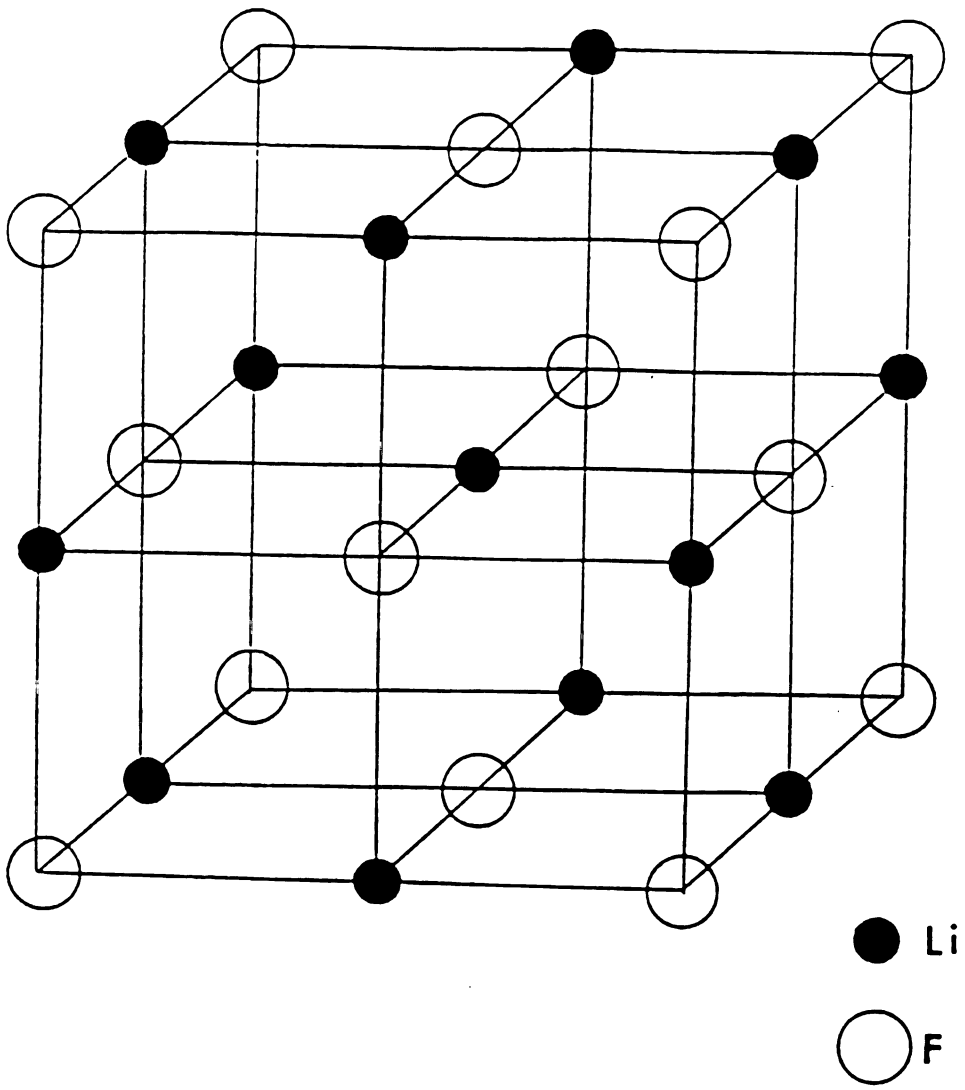

Figure.2 Crystal Structure of Lithium Fluoride, from [29].

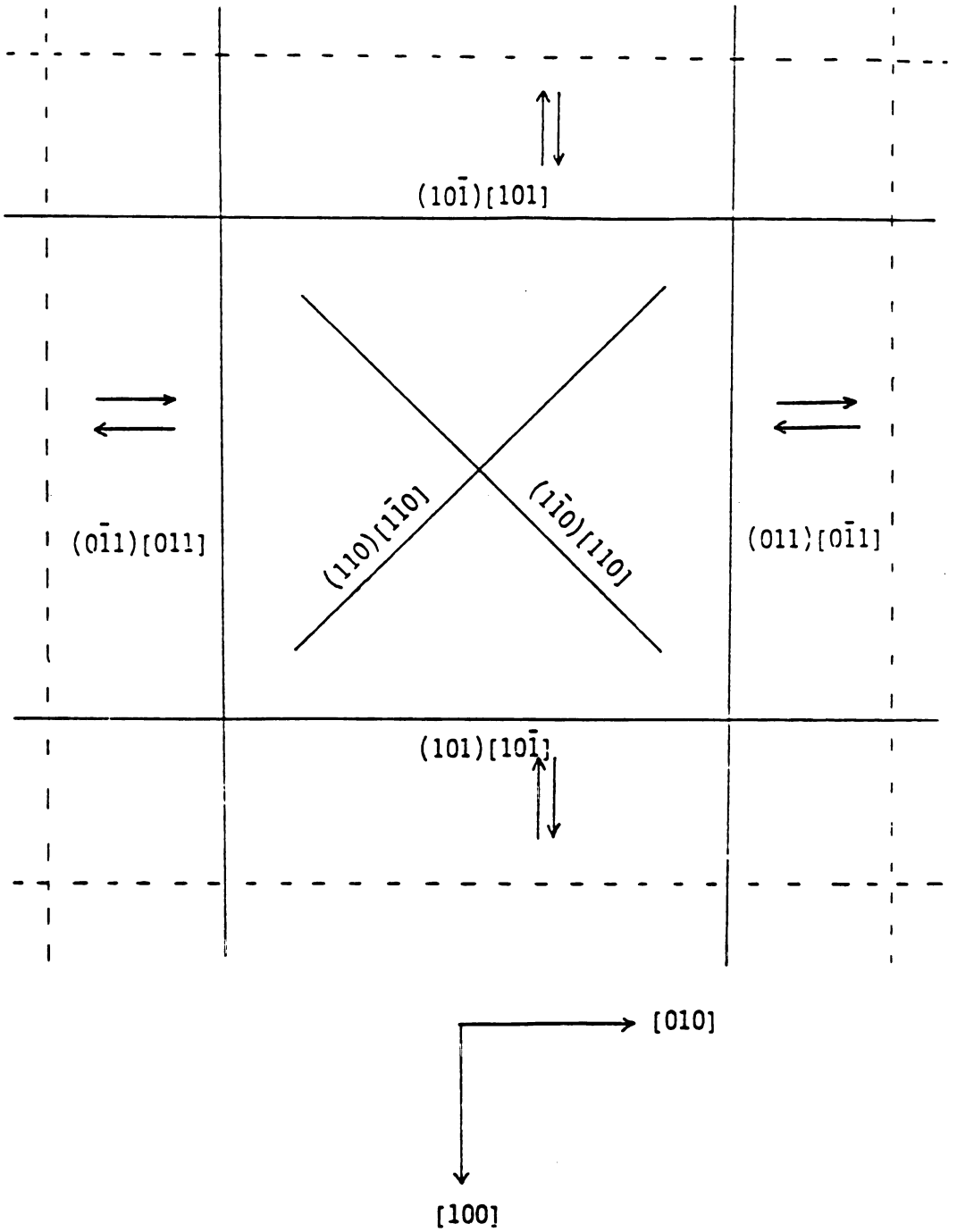

Figure.3 Projection of {110} Slip Planes onto (001) Surface of Lithium Fluoride Crystal, from [30].

{111}<110>, while at low temperatures, rock salt structures have only two independent slip systems within the slip systems $\{1\bar{1}0\}<110>$ [31].

Lithium Fluoride, in its brittle state, fractures by cleavage along specific crystallographic planes. Primary cleavage occurs along the {100} planes and secondary cleavage occurs along the $\{1\bar{1}0\}$ planes [32]. Anisotropy of surface energies in crystals with strong cleavage tendencies dictates the crack path [29]. Fracture, in single crystals, usually occurs along planes having the lowest fracture surface energy [31].

Cleavage along primary and secondary cleavage planes occured during laser processing of both the {100} and $\{1\bar{1}0\}$ surfaces of LiF single crystals using a continuous wave CO_2 laser [28]. It was suggested that secondary cleavage occured to relieve the high thermal stresses. This was due to the limited number of primary cleavage planes in LiF [28]. Surface damage around the melt zone consisted of cracks compromising between crystallographic cleavage planes and non-crystallographic planes. This was attributed to thermal stresses. This study also showed the existence of cleavage steps indicating discontinuous crack propagation. The crack stopped and restarted repeatedly [28].

Etching techniques applied to the LiF single crystals indicated that cracking did not occur due to the interaction of dislocations. A mechanism based on thermal stresses was

more probable since no plastic deformation occured prior to fracture [28]. The process of laser heating, at high laser fluences, is probably too fast to allow plastic deformation to occur. The high concentration of energy was brought by the laser induced large stresses. The thermal stresses were thought to be relieved by cracking before any plastic deformation took place [28]. It was suggested that at very high temperatures, when the lattice vibrations (phonons) have a high frequency, they act as barriers to dislocation motion. Plastic deformation is then more dificult than at low temperatues [33]. Fracture before the occurrence of plastic deformation is typical of brittle crystals. Chaudri et al., on the other hand, studied the effect of impact erosion on single crystals of NaCl, MgO, and LiF [34]. They noted that at high strain rates, the crystals behaved in a brittle fashion. They also registered a linear increase in the dynamic hardness as the strain rate increased.

Lee [29] used bicrystals of LiF to compare the effects of Impact erosion and Quasi-static identation on the fracture and deformation behavior of bicrystals. He suggested that the most important contact parameters that affect the mode and extent of damage produced by particle impact were the pressure, the contact radius, and the contact time. The pressure controlled the extent of elastic and plastic deformation of the material, the contact radius related the pressure or stress to the applied force while

the contact time determined the force history [29].

Comparing contact parameters such as contact time, pressure induced by the particle and the contact radius for impact erosion with those of pulsed-laser processing, the most important parameters for pulsed-laser processing are the pulse length, the energy per pulse, and the beam diameter. These three parameters are essential for estimating the laser-induced pressures on the surface and the bulk material as shown from equations (6) and (7). The pressures control the mode and extent of deformation in the material.

The aim of this project is to study and assess the laser-induced damage due to thermal stresses caused by laser irradiation on the (001) faces of LiF single crystals. The transparency of lithium fluoride permits the observation of various types of damage on the surface and inside the bulk.

II. EXPERIMENTAL APPARATUS

The CO_2-laser used during this work was a TLF 2500 made by the TRUMPF INC. It generates invisible laser light at 10.6μm wave length with a maximum power of 2500 watts. The laser power output consistency is about ±2%. This laser can be operated either in a continuous mode or a pulsed mode.

The laser machine includes four main components as shown in Figure.4.

1) The laser control Tcc: Figure.5 is a schematic of the three main components of the laser control. (i) is a portable operating panel with graphic electronic display and sealed keyboard. (ii) is a modular micro-computer card system. (iii) is the wiring board to connect the card system with the periphery.

2) H.F: The H.F generates high frequency electrical energy. The frequency is 13.56 MHz and is maintained at a constant rate by an oscillator stage. The output of the oscillator stage is amplified by intensifier circuits and sent to the beam generator through a coaxial cable.

3) Beam generator (resonator and supply). The resonator includes a vacuum pump, roots pump and a gas mixing unit.

4) Cooling units. The laser contains two cooling units. The two units offer two setting possibilities for the desired temperature. They are responsible for cooling two different circuits, one for Copper made components and the other for Aluminum made components.

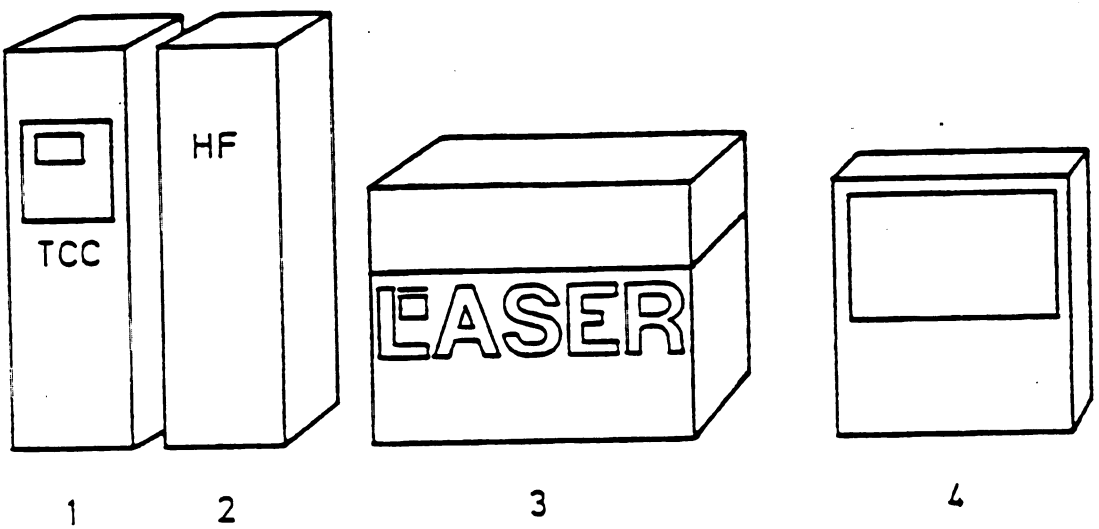

Figure.4 Schematic Representation of Main Components of the Laser: (1) is the Laser Control Tcc, (2) is the H.F, (3) is the Beam Generator, and (4) is the Cooling Unit.

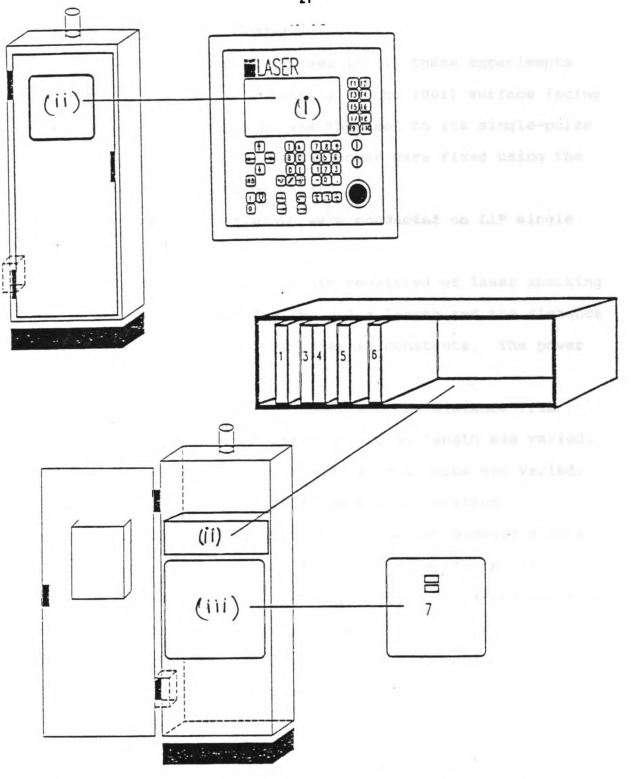

Figure.5 Tcc Components: (i) is the Operating Panel, (ii) is a Modular Microcomputer Card System, and (iii) is the Wiring Board.

III. EXPERIMENTAL PROCEDURE

The LiF single crystals used in all these experiments were set on a metallic support with the (001) surface facing the laser head. The laser was then set to its single-pulse mode. The pulse length and the power were fixed using the keyboard on the operating panel.

Five sets of experiments were conducted on LiF single crystals.

A. The first set of experiments consisted of laser shocking the single crystal keeping the pulse length and the distance from the focal point of the laser as constants. The power was the only variable.

B. For The second set, the power and the distance from focus were kept constant while the pulse length was varied.

C. For the third set, the distance from focus was varied. The power and the pulse length were kept constant.

D. The fourth set consisted of etching the damaged single crystals with a very dilute solution of ferric chloride. Etching time lasted from 12 to 16 seconds. Dislocation etch pits produced by this method revealed the slip distribution. This is to show the extent of plastic deformation due to the laser-induced thermal stresses on the (001) surfaces of the LiF single crystals.

E. The purpose of the fifth set of experiments was to reveal the role of the sample thickness on the crack propagation and the extent of the laser damage. The width

of the heat affected zone and the maximum length of cracks were then recorded.

All observations and analysis relating to the above experiments were made using reflected light microscopes and the scanning electron microscope. The micrographs taken on the (001) surfaces of the LiF single crystals and the schematics representing the laser damage on these surfaces were all bounded by the <100> directions at the bottom and top, and the <010> directions at the right and left sides. The diagonals have the <110> directions.

IV. RESULTS AND DISCUSSION

A. Laser Damage as a Function of Laser Power.

During this experiment the laser pulse length and the distance from the laser focal point were kept constant. The laser power was decreased from treatment.1 to treatment.3. The sample dimensions were 37 mm x 14.5 mm x 3.5 mm.

1) Treatment.1

The pulse length was t=340 ms.

The laser power was P=190 watts.

The beam area at the focal point was A=0.245 mm^2 .

The energy density calculated at the surface is:

$$I = tP/A = 2.63 \times 10^4 \text{ joules/cm}^2$$

a) A well-defined damaged zone (D.Z) can be seen in Figures 6,7,and 8. This area with width equal to 1.35mm, included a crater in the middle. This is where material had melted and resolidified. The crater area is just larger than the beam area. Observation of the S.E.M micrographs given in Figures 8,9 and 10 indicated the occurrence of melting and probable evaporation. The crater shown in Figure.8 contains pores that may have started as gas bubbles underneath the surface and exploded. This is a sign of evaporation.

The area surrounding the crater consisted of material pushed from the bulk onto the surface. This material could

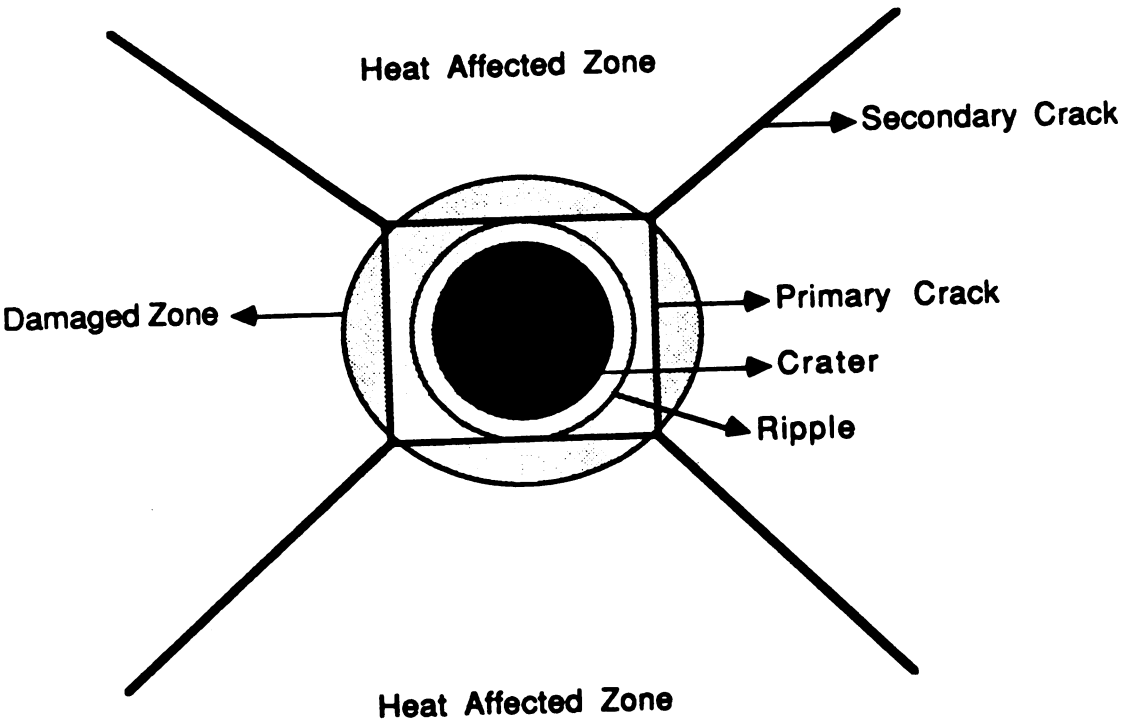

Figure.6 Schematic Showing the Laser Damage for Treatment.1, (Power = 190 Watts and Fluence = 2.63×10^4 Joules/cm^2).

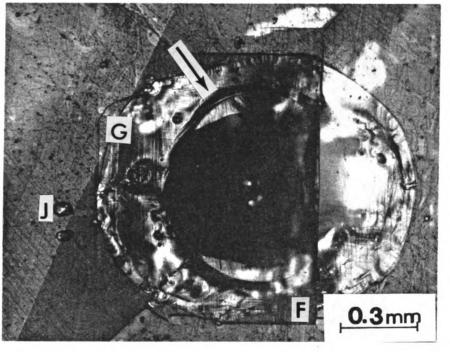

Figure.7 Optical Micrograph Showing the D.Z for Treatment.1.

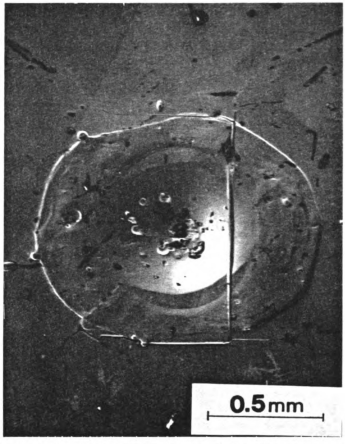

Figure.8 S.E.M Micrograph Showing the D.Z for Treatment.1

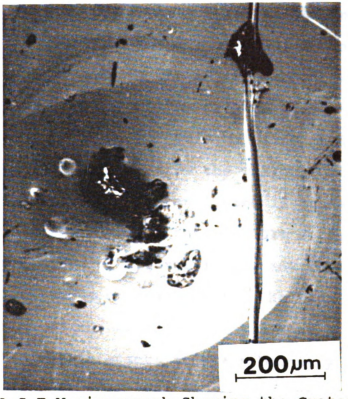

Figure.9 S.E.M micrograph Showing the Crater Area for Treatment.1.

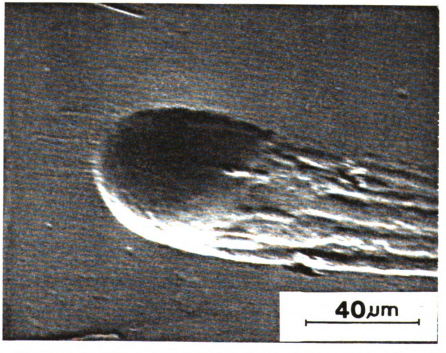

Figure.10 S.E.M Micrograph Showing an Evaporation Site on the surface for Treatment.1.

be a compensation for the crater material pushed into the bulk. Edges of the damaged zone are shown by the arrows in Figures 11 through 14. The material in the D.Z had been stacked above the surface as can be observed by the difference in height between the D.Z edges and the heat affected zone (H.A.Z). This may also be due to molten material flowing away from the crater. The material from the D.Z as seen in Figures 11 and 13 descended towards the H.A.Z in steps parallel to the (001) surface.

Observation of Figures 12,13, and 14 indicate non-crystallographic cracks bounding the D.Z in some areas. The separation of the D.Z from the H.A.Z as observed by the non-crystallographic cracks at their boundary can be due to high tensile stresses exerted on the D.Z during the cooling phase of the laser heating process.

Ripples at the edge of the resolidified area in the middle of the D.Z were shown by the arrows in Figures 7, and 8. Ripples can be a result of plastic deformation caused by slip. Slip can occur due to the compressive thermal stresses acting during the laser heating of the surface.

b) Primary (100) and secondary (110) cleavage cracks were observed. They are connected directly to each other, or through non-crystallographic cracks.

c) Primary cleavage cracks were seen to jump from one (100) plane to another parallel (100) plane as they propagate.

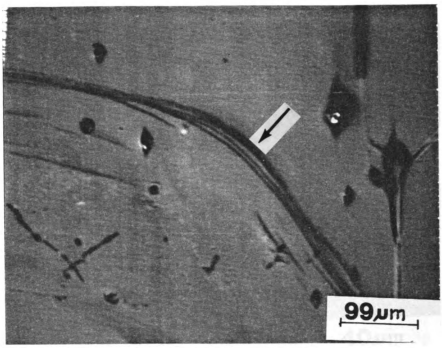

Figure.11 S.E.M Micrograph Showing the Edge of the D.Z for Treatment.1.

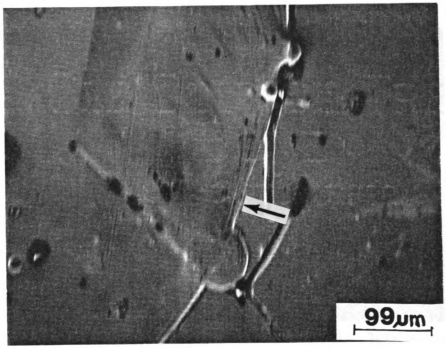

Figure.12 S.E.M Micrograph Showing Cracks Bounding the D.Z for Treatment.1.

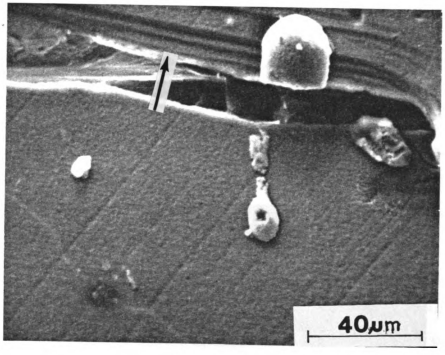

Figure.13 S.E.M Micrograph Showing the Edge of the D.Z for Treatment.1.

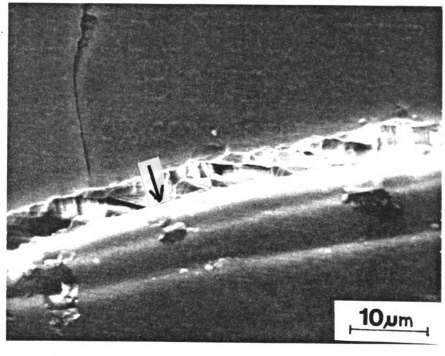

Figure.14 S.E.M Micrograph Showing the Edge of the D.Z Noted by the star in Figure.8.

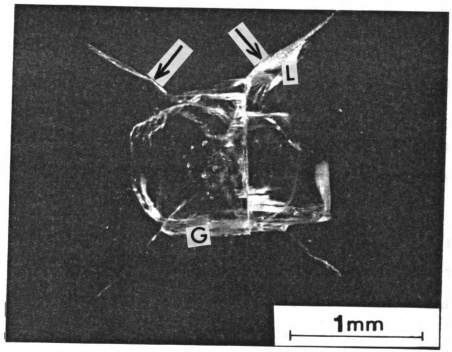

Figure.15 Laser Damage Observed Inside the Bulk of the LiF Single Crystal for Treatment.1.

Steps were observed on the surface as shown by the letter (F) in Figure.7 and into the bulk as shown by the letter (G) in Figure.7 and Figure.15. The cleavage steps form in LiF when the crack velocity falls below the critical value for which the density of nucleated dislocations at the crack tip increases with decreasing crack velocity. When the crack intersected screw dislocations, the leading edge of the crack became jagged and cleavage steps were formed as the crack continued its propagation [35].

d) Secondary (110) cracks started from the damaged zone (D.Z) as non-crystallographic cracks shown by arrows in Figure.15. Deviations from the crystal cleavage directions can be due to competition between natural crystallographic cleavage and thermal stress direction effects. Non-crystallographic cracks usually propagated in planes that were not perpendicular to the (001) surface. They induced shaded areas in these micrographs similar to the ones indicated by (L) in Figure.15.

e) Splattered material was observed on the surface. This was shown by the letter (J) on the left side of the D.Z shown in Figure.7.

2) Treatment.2

For this treatment t=340 ms, P=163 watts, A=0.245 mm^2, and I=2.26x10^4 J/cm^2.

a) The D.Z for treatment.2 was smaller in area than in

treatment.1. Its width or maximum diameter was 1.18mm and its shape was very similar to that of treatment.1 where material had emerged from the bulk and stacked on the surface. This can be seen in the S.E.M micrographs presented in Figures 16,17, and 18.

b) Primary and secondary cleavage cracks were observed. They are usually connected by non-crystallographic cracks as shown by the arrows in Figures 19 and 20 .

c) Primary cleavage steps were observed as shown in Figure.20. The stepping in (100) crack propagation was not as abundant as it was for treatment.1.

d) Ripples at the rim of the resolidified area in the D.Z were observed. These are shown by the arrow in Figure.17.

e) Secondary cracks were considerably shorter than in treatment.1. This may indicate a lower driving force for secondary crack propagation in treatment.2.

3) Treatment.3

Treatment.3 was repeated three times in order to get reasonable results. This was due to fluctuations of up to 10% in power which was present during low power (around 100 watts) laser treatments.

For this treatment t=340 ms, P=125 watts, A=0.245 mm^2 and $I=1.73x10^4$ J/cm^2.

a) The D.Z shown in Figures 21 and 22 had width equal to 1.01mm. The area on the surface coinciding approximately

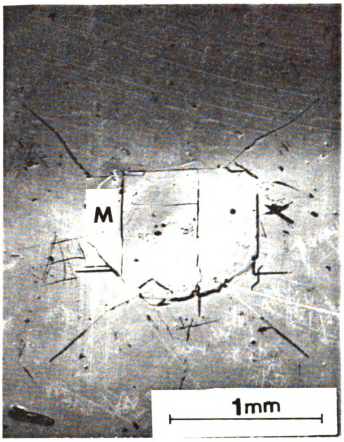

Figure.16 S.E.M Micrograph Showing the Laser Damage for Treatment.2, (Power = 163 Watts and Fluence = 2.26×10^4 Joules/cm^2).

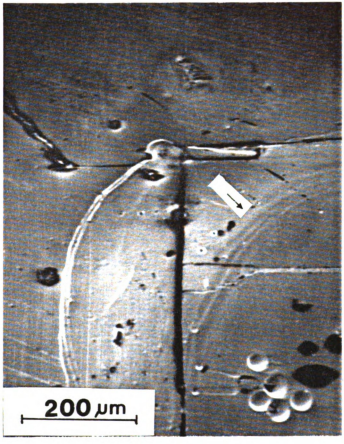

Figure.17 S.E.M Micrograph Showing a Corner of the D.Z for treatment.2. (This is Marked by (M) in Figure.16).

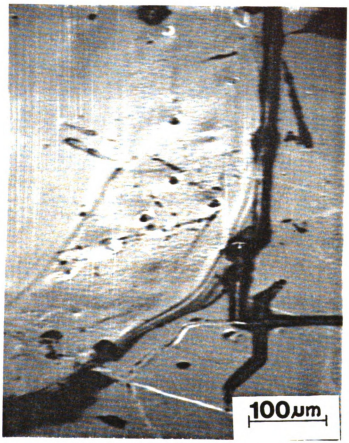

Figure.18 S.E.M Micrograph Showing a Crack Bounding the D.Z for Treatment.2.

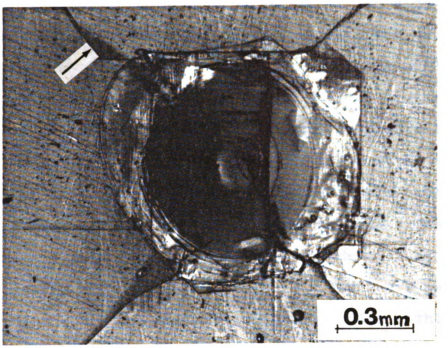

Figure.19 Optical Micrograph Showing the D.Z for Treatment.2.

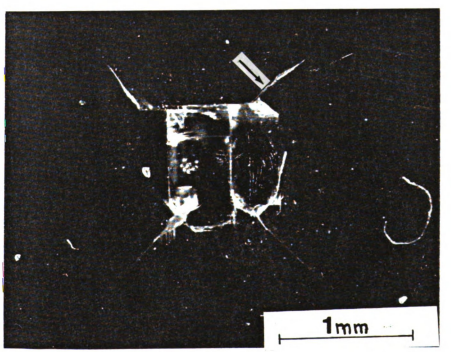

Figure.20 Optical Micrograph Showing the Damage Inside the Bulk for Treatment.2.

with the beam area was 0.7mm in width. No sign of melting could be observed in this area. Melting may have been very minor and included only a thin layer of the surface. Few ripples at the edge of the melted zone or crater were observed and are marked by the arrow in Figure.21.

The ripple pattern observed in the central area of the crater in Figure.21 was called helix ripple pattern so as to differentiate it from the ripples observed around the crater. This ripple pattern will be denoted by H.R.P in the following sections of this thesis. The H.R.P seen for treatment.3 had a diameter equal to 0.25mm. This is only about one third of the diameter of the crater. This macroscopic type of laser damage was found in several following laser-treatments also. Its mechanism of formation is not fully understood. However, possible mechanisms that could cause this are discussed in a later section of this thesis.

The edges of the D.Z, on the other hand, are marked by the arrows in Figures 23,24, and 25. They were bounded by non-crystallographic cracks as seen in the case of earlier treatments with higher laser power.

b) Only one very short (0.2 mm) secondary crack was observed. This was marked by the letter (N) in Figure.21. At this very low energy density, primary cleavage is the only type of cleavage induced by laser thermal energy.

c) Cleavage steps were also observed. They were shown by

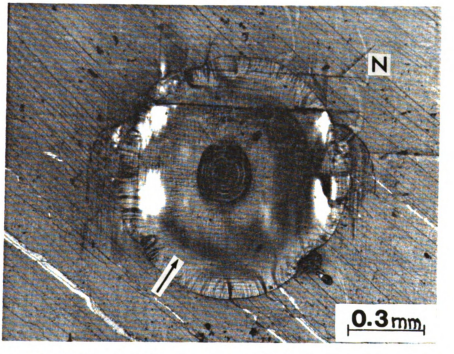

Figure.21 Optical Micrograph Showing the Laser Damage for Treatment.3,4 (Power = 125 Watts and Fluence = 1.73 10^4 Joules/cm^2).

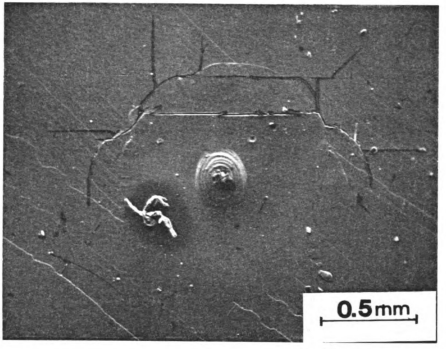

Figure.22 S.E.M Micrograph Showing the Laser Damage for Treatment.3.

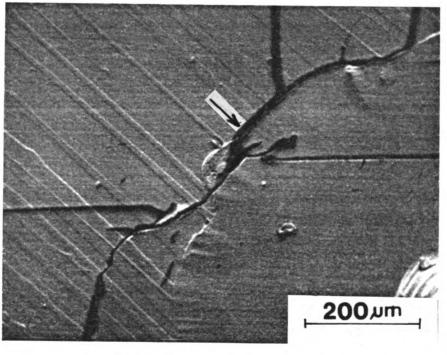

Figure.23 S.E.M Micrograph Showing Cracks Bounding the D.Z for Treatment.3.

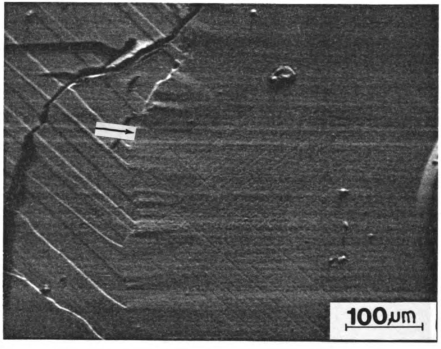

Figure.24 S.E.M Micrograph Showing the Boundary between the D.Z and the H.A.Z for Treatment.3.

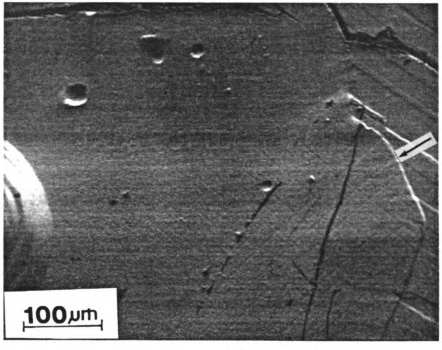

Figure.25 S.E.M Micrograph Showing the Boundary between the D.Z and the H.A.Z for Treatment.3.

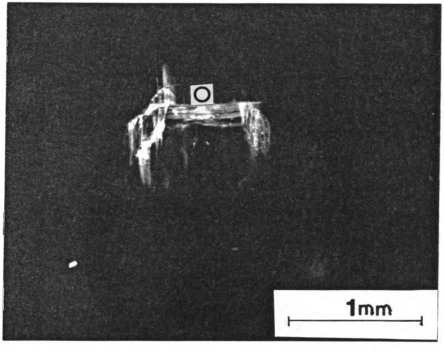

Figure.26 Optical Micrograph Showing the Laser Damage as seen Inside the Bulk for Treatment.3.

the (O) in Figure.26.

The schematic given in Figure.27 is a comparison of the shapes of the D.Z's for treatments 1,2, and 3. Increasing the power has shown to induce deeper craters and more material is pushed onto the surface.

A summary of the laser parameters and the laser-induced damage as indicated by the D.Z width and the length of the cleavage cracks for treatments 1 through 3 are presented in Table.1.

B. Laser Damage as a Function of Laser Pulse Length

During this experiment, the laser power and the distance from the focal point were kept constant. The laser pulse length was decreased from treatment.4 to treatment.6 so that the energy densities correspond respectively with those of treatment.1 through treatment.3. The sample dimensions were 37 mm x 14.5 mm x 3.5 mm.

1) Treatment.4

For this treatment, t=540 ns, P=120 watts, A=0.245 mm^2 and I=2.64×10^4 J/cm^2.

a) The width of the D.Z in treatment.4 was 2.4 mm as compared to only 1.35 mm in treatment.1 with the same energy density. Its shape was almost flat as shown in Figure.28. Since the laser-contact time with the surface (pulse length)

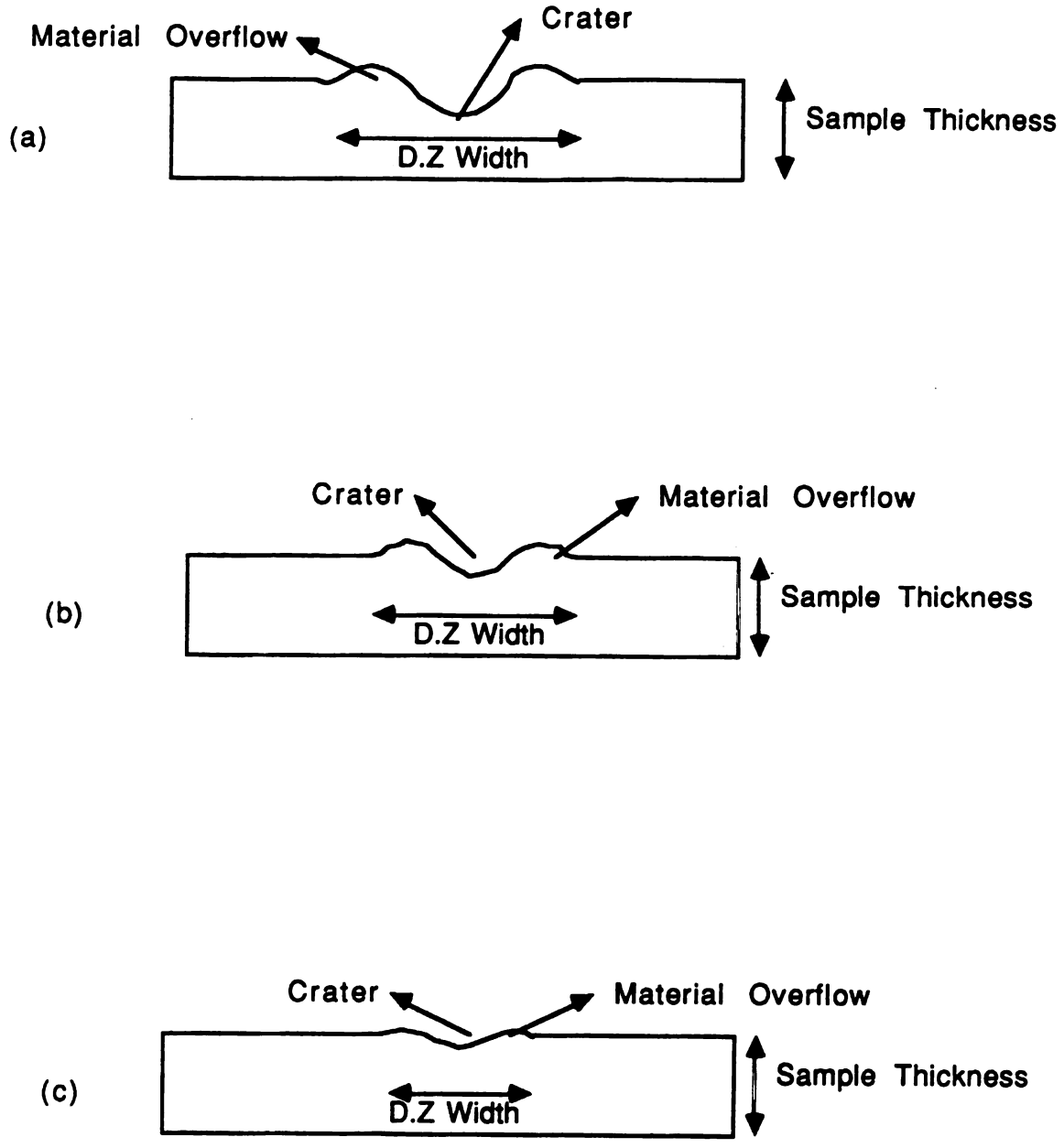

Figure.27 Schematic of Laser Damage as a Function of Laser Power. (a) Shape of the D.Z for Treatment.1, (b) Shape of the D.Z for Treatment.2, and (c) Shape of the D.Z for Treatment.3.

Table.1: Summary of the Results Obtained for Increasing Laser Power from Treatment.1 to Treatment.3.

	Treatment.1	Treatment.2	Treatment.3
Pulse Length (ms)	340	340	340
Power (watts)	190	163	125
Distance From Focus (mm)	0.0	0.0	0.0
Energy Density (10^4 Joules/cm^2)	2.63	2.26	1.73
D.Z Width (mm)	1.35	1.18	1.01
Length of The Longest Secondary Cleavage Crack (mm)	1.23	0.72	0.2
Length of The Longest Primary Cleavage Crack (mm)	1.14	1.10	1.10

was long, the material from the bulk had moved over a larger area.

The helix ripple pattern (H.R.P) can be seen around the center of the crater in Figure.29. Also, in the center of the crater, material had recrystallized slowly in crystallographic shapes. This can be seen in the S.E.M micrograph of Figure.30. Radial striations around this central area were also seen (Figure.29). These may have been left behind by the molten material flow from the center of the crater.

b) Primary and secondary cleavages were observed. They are very well defined straight lines in most cases.

c) The length of secondary (110) cracks reached up to 3.25 mm from inside the D.Z as compared to 1.2 mm for treatment.1 with the same energy density.

d) Primary cleavage steps were observed. They are shown by the arrows in Figures 31 and 32. Cleavage steps can also be seen from the back of the sample as illustrated in Figure.33.

e) Cracks in treatment.4 were much wider (about 10 times) than cracks observed in treatment.1. (Compare Figure.7 and Figure.29).

Comparing treatment.1 and treatment.4, both with the same energy density of 2.6×10^4 J/cm^2, it can be concluded that the time of laser contact with the surface was very

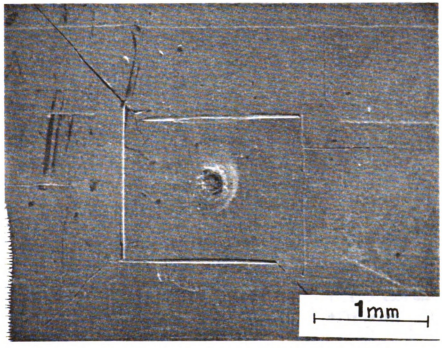

Figure.28 S.E.M Micrograph Showing the Laser Damage for Treatment.4, (Pulse Length = 540 ms and Fluence = 2.64×10^4 Joules/cm^2).

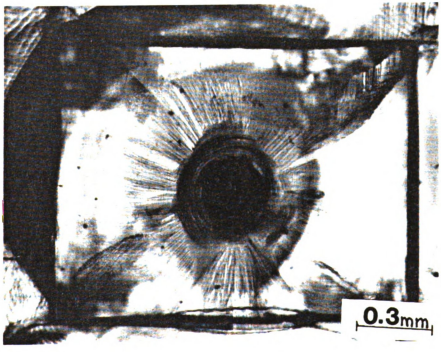

Figure.29 Optical Micrograph Showing the Laser Damage in the Crater Area for Treatment.4.

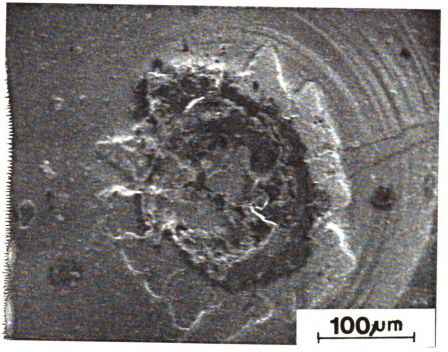

Figure.30 S.E.M Micrograph Showing Recrystallization in the Crater Area for Treatment.4.

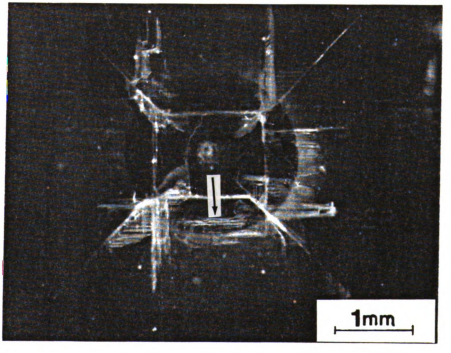

Figure.31 Optical Micrograph Showing the Laser Damage Inside the Bulk for Treatment.4.

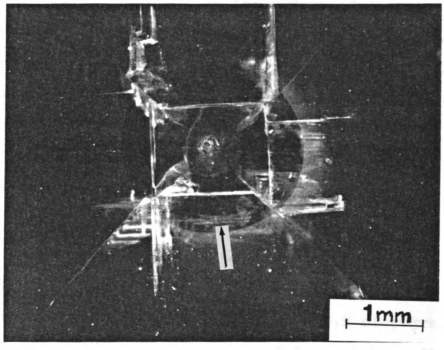

Figure.32 Optical Micrograph Showing the Laser Damage Inside the Bulk for Treatment.4.

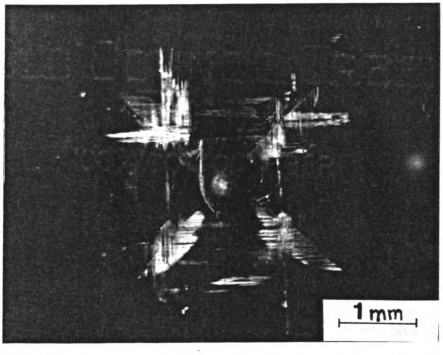

Figure.33 Laser Damage for Treatment.4 as seen from the Back of the Sample.

critical in determining the extent of damage. Longer pulse lengths induced slower accumulation of the damage which resulted in much longer secondary cleavage cracks, much wider cracks, and much wider D.Z in treatment.4 as compared to those for treatment.1.

2) Treatment.5

For this Treatment t=460 ms, P=120 watts, A= 0.245 mm^2, and I=2.25x10^4 J/cm^2.

a) The damaged zone had a width equal to 1.95 mm and can be seen in Figures 34 and 35. The S.E.M micrograph shown in Figure.36 indicated that the D.Z was not as flat as that of treatment.4. This was due to this treatment's lower pulse length. The crater area was larger than the beam area. The crater is indicated by the arrows in Figure.36. Radial striations are also seen and noted by the letter (S) in Figure.36. Ripples around the crater can also be observed in this Figure.

b) Primary and secondary cleavage cracks were present. Non-crystallographic cracks were observed in treatment.5 as opposed to treatment.4.

c) Cleavage steps were observed. They are indicated by the letter (P) in Figures 34 and 36.

d) Secondary cracks observed for this treatment are shorter than for treatment.4. The longest crack measured 2.35 mm as opposed to 3.25 mm in treatment.4. Note that the length of

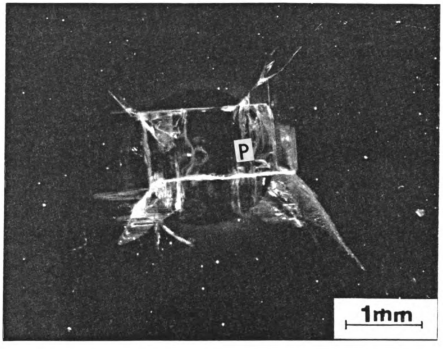

Figure.34 Optical Micrograph Showing the Laser Damage for Treatment.5, (Pulse length = 460 ms and Fluence = 2.25×10^4 Joules/cm^2).

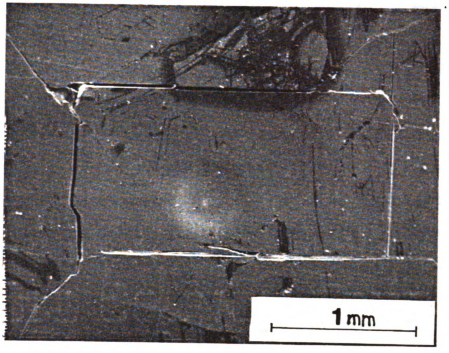

Figure.35 S.E.M Micrograph Showing the D.Z for Treatment.5.

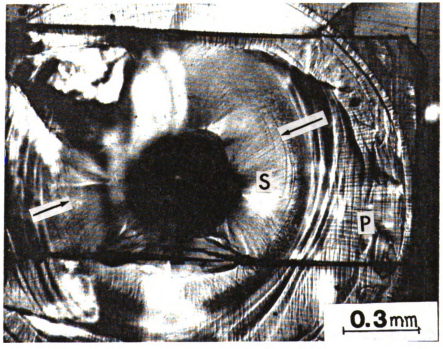

Figure.36 Optical Micrograph Showing the D.Z for Treatment.5.

primary cracks, especially those that started within the D.Z, did not depend on the energy density. This was observed by comparing treatments 1 through 3 and also by comparing treatments 4 and 5. Secondary cleavage was predominant for treatments 1, 2, 4, and 5. Its propagation was driven by the high energy densities provided by lasers. Primary cracks seemed to reach towards a stable, maximum length. More energy or driving force for crack propagation appears to contribute mostly towards the extension of secondary cracks.

3) Treatment.6

For this treatment t=380 ms, P=120 watts, A=0.245 mm^2 and I=1.86x10^4 J/cm^2.

a) The D.Z of treatment.6 had a width equal to 1.62 mm. The D.Z, as seen in the S.E.M micrograph given in Figure.37, had a much deeper crater and more overflown material as compared to the higher pulse-length treatments of this set of experiments. Ripples around the crater can be observed in Figure.38. This Figure does not indicate the existence of radial striations observed in some of the earlier treatments.

b) No trace of secondary cracks were observed for this treatment. The two primary cleavage cracks are perpendicular to each other and intersect at the center of

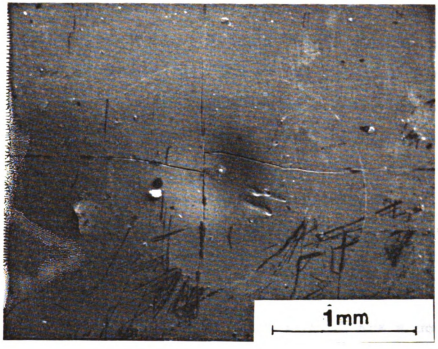

Figure.37 S.E.M Micrograph Showing the Laser Damage for Treatment.6, (Pulse Length = 380 ms and Fluence = 1.85×10^4 Joules/cm^2).

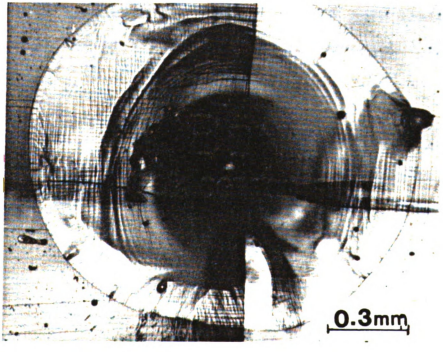

Figure.38 Optical Micrograph Showing the D.Z for Treatment.6.

the D.Z. This can be seen in Figure.39. This set of primary cracks has never been observed in any of the five earlier treatments. Primary cracks inside the D.Z usually form a rectangle with its center coinciding with the center of the D.Z. These cracks never crossed the center of the damaged zone. This set of cracks, intersecting at the center (molten zone) indicates that cracking may have occured during the resolidification process.

c) Cleavage steps were observed. This is shown by the arrows in Figure.39.

The shematics given in Figure.40 are a comparison of the D.Z's shapes for treatments 4 through 6. The increasing depth of the crater and amount of overflown material from treatment.4 to treatment.6 indicated the effect of decreasing the pulse-length. The decreasing of laser-contact time with the surface induced more limited propagation of the damage. Damage propagated over smaller areas.

A summary of the laser parameters and the laser damage as indicated by the D.Z width and the length of the cleavage cracks for treatments 4 through 6 is presented in Table.2.

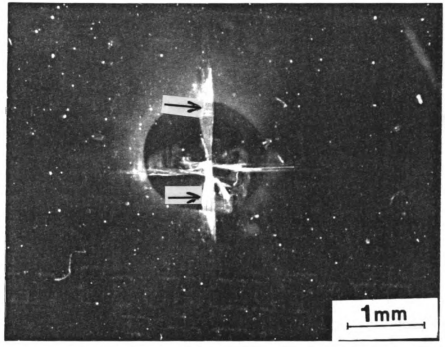

Figure.39 Optical Micrograph Showing the Laser Damage Inside the Bulk for Treatment.6.

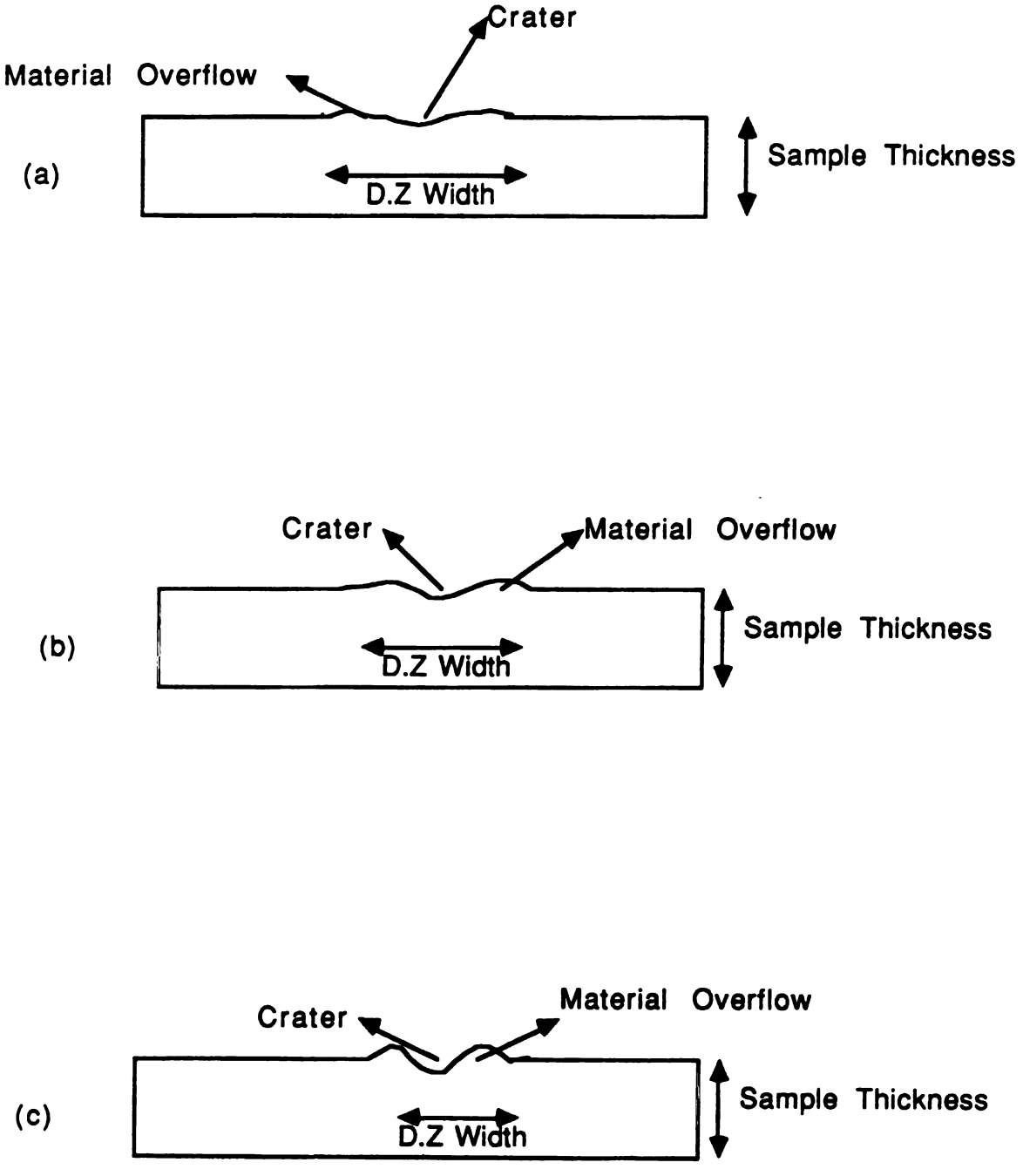

Figure.40 Schematic of the Laser Damage as a Function of the Pulse Length. (a) Shape of the D.Z for Treatment.4, (b) Shape of the D.Z for Treatment.5, and (c) Shape of the D.Z for Treatment.6.

Table.2: Summary of the Results Obtained for Increasing the Pulse Length from Treatment.4 to Treatment.6.

	Treatment.4	Treatment.5	Treatment.6
Pulse Length (ms)	540	460	380
Power (watts)	120	120	120
Distance From Focus (mm)	0.0	0.0	0.0
Energy Density (10^4 Joules/cm^2)	2.64	2.25	1.86
D.Z Width (mm)	2.40	1.95	1.62
Length of The Longest Secondary Cleavage Crack (mm)	3.25	2.35	0.00
Length of The Longest Primary Clevage Crack (mm)	1.5	1.85	2.35

C. Laser Damage as a Function of Change in the Distance From the Laser Focal Point to the Surface.

During this set of experiments the laser power and pulse length were kept constant. The distance from the laser focal point was increased gradually from treatments 7 and 8 to treatment.10. The distances from the focal point were calculated using a plot of the beam diameter versus the distance from focus for a ten inch lens. The energy densities of treatments 8 through 10 corresponded respectively with those of treatments 1 through 3 and also treatments 4 through 6. The sample used was relatively thin and had dimensions equal to 37 mm x 14.5 mm x 1.3 mm. Note that very thin samples, as was found in set E of experiments, would result in more extensive damage on the surface as well as inside the bulk. This factor has to be taken into account when analysing the results of treatments 7 through 10.

1) Treatment.7

For this treatment t=400 ms, P=190 watts, A=0.275 mm^2 which corresponded to a distance from the focal point d=6.86 mm. The energy density was I=2.76x10^4 J/cm^2.

a) The D.Z in this treatment was very clear since no cracks were present. This can be seen in figures 41,42, and 43 where the D.Z was a perfect circle as opposed to the other treatments. The diameter of the circle was 0.96 mm. Inside

the D.Z, the crater, which was the area just larger than the beam area, had width equal to 0.7mm. The edge of the crater was shown by the arrows in Figures 41 and 43.

The helix ripple pattern (H.R.P) was also observed as shown in Figures 41,42, and 43. The H.R.P width (0.4mm) was smaller than the beam dimeter on the surface (0.6mm).

The radial striations observed in earlier treatments can also be observed around the H.R.P of treatment.7. They are marked by the (R) in Figure.43.

b) No cracking had occurred during this treatment with approximately the same energy density as treatment.1 and treatment.4. This proves that the amount of damage induced by laser is not only dependent on the energy density but also very dependent on the extent of the different laser variables (power, pulse length, and distance from focus).

c) Primary 45^{o} (110) slip traces were observed around the D.Z. They are noted by the letter (W) in Figure.43.

2) Treatment.8

For this treatment the pulse length was increased and the power was decreased as compared to treatment.7. The distance from the focal point, and the energy density were kept constant. This was carried out in order to induce cracking in the sample. It was noted from the previous experiments that the pulse length, among other laser variables had the most critical effect on the extent of the

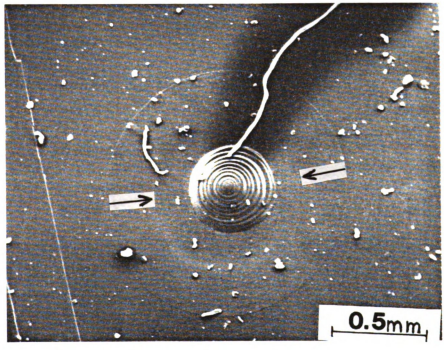

Figure.41 S.E.M Micrograph Showing the D.Z for Treatment.7, (Pulse Length = 400 ms, Distance from focus = 6.9 mm, and fluence = $2.76X10^4$ Joules/cm^2).

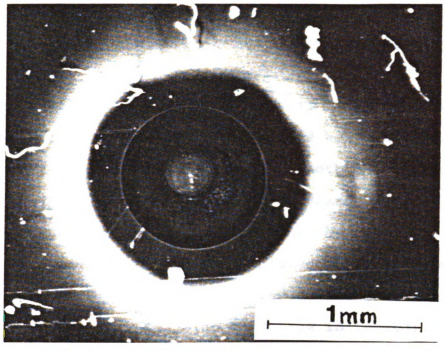

Figure.42 Optical Micrograph Showing The D.Z for Treatment.7.

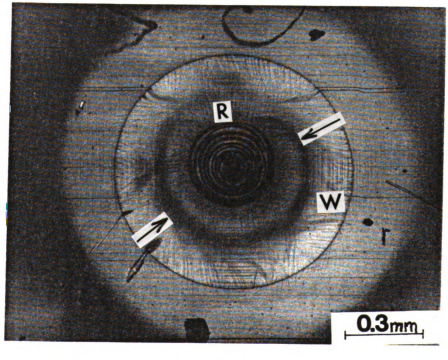

Figure.43 Optical Micrograph Showing the D.Z for Treatment.7. Different Lightening than for Figure.42.

damage induced by laser.

For Treatment.8, t=500 ms, P=151 watts, d=6.86 mm, so A=0.275 mm^2, and I=2.75x10^4 J/cm^2.

a) The width of the D.Z was 2.13 mm as compared to 0.96 mm for treatment.7. This indicated again the significant influence of the laser pulse length and the small thickness of the sample on the extent of damage induced. A crater with a H.R.P in the center could be observed in Figure.44.

b) Primary and secondary cleavages were present as can be seen in Figure.45. Primary cleavage cracks were predominant and were very long (up to 5.2 mm in length). This can be seen in Figure.44. They went very deep inside the bulk and reached the back of this thin sample.

c) Cleavage steps were left behind primary cleavage cracks as can be observed in Figures 44 and 46.

3) Treatment.9

For this treatment t=500 ms, P=151 watts, d=8.9 mm, so A=0.319 mm^2, and I=2.36x10^4 J/cm^2.

Features in this treatment were similar to those in treatment.8, except smaller. (Compare Figure.44 and Figure.47).

a) The diameter (width) of the D.Z was 2.2 mm. A crater with a H.R.P in the center can be observed in Figure.47.

The radial striations, believed to be left behind by

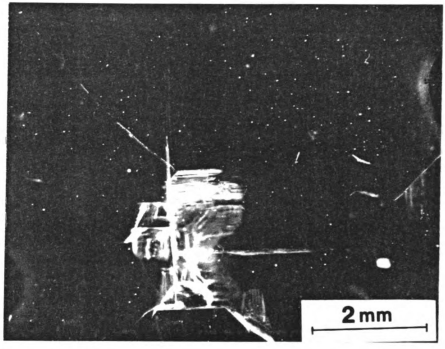

Figure.44 Optical Micrograph Showing the Laser Damage for Treatment.8, (Distance from Focus = 6.9 mm and Fluence = 2.74×10^{4} Joules/cm^{2}). .

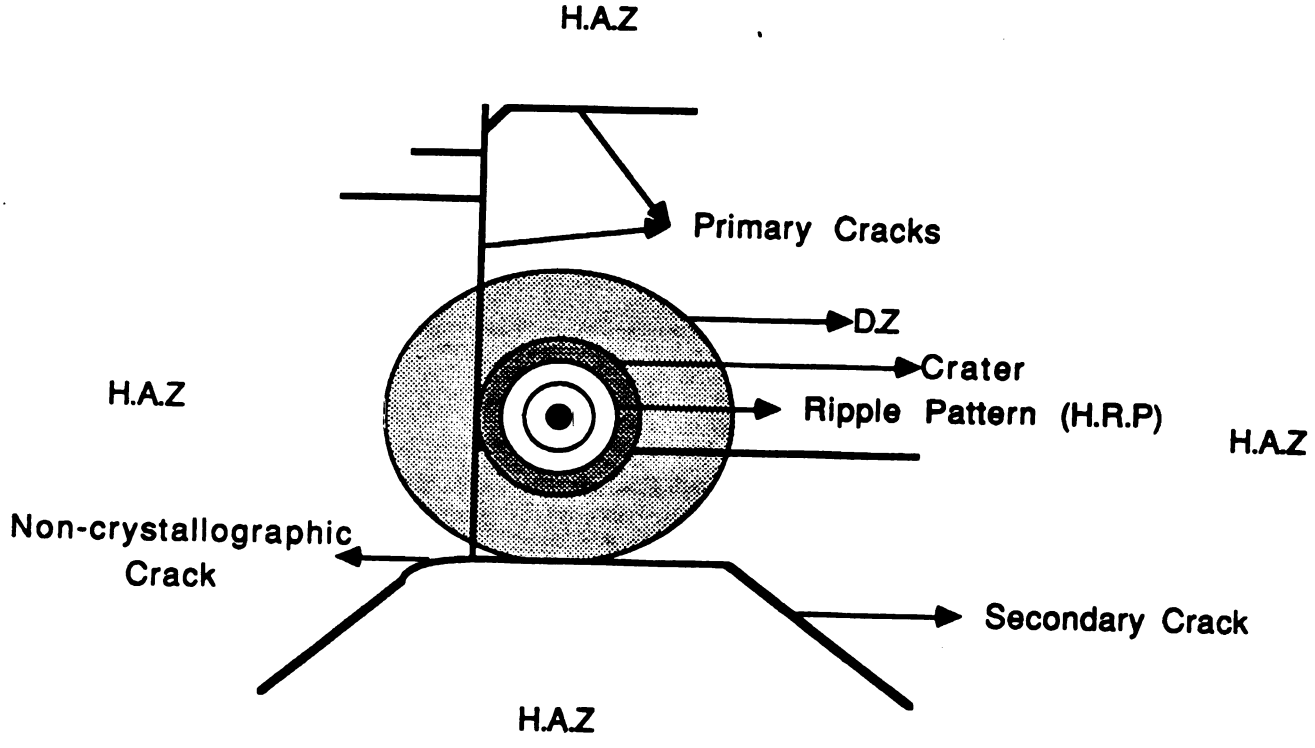

Figure.45 Schematic Showing the Laser Damage for Treatment.8.

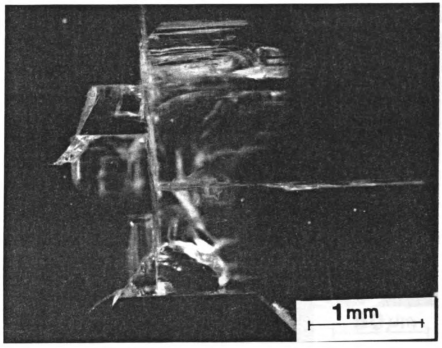

Figure.46 Optical Micrograph Showing the Laser Damage Inside the Bulk for Treatment.8.

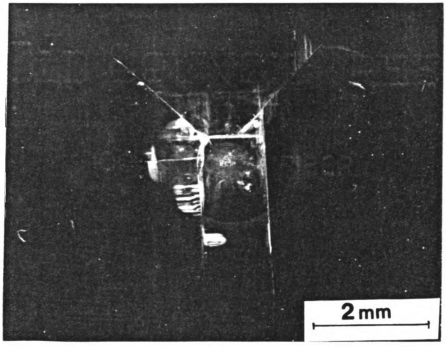

Figure.47 Optical Micrograph Showing the Laser Damage Inside the Bulk for Treatment.9, (Distance from Focus = 8.9 mm and Fluence = 2.36×10^4 Joules/cm^2).

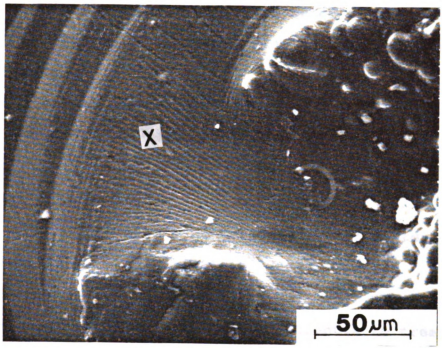

Figure.48 S.E.M Micrograph Showing Radial Striations as Seen Around the Center of the Crater for Treatment.9.

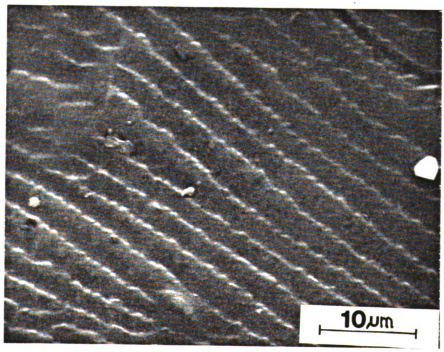

Figure.49 Magnified View of Region (X) Shown in Figure.48.

molten material flow from the center of the crater, can be seen in figure.48. They were noted by the letter (X) in this Figure. A magnified view of this area is provided in Figure.49.

b) Primary cracks reached up to 3.7 mm in length. Secondary cracks reached 2.4 mm in length.

4) Treatment.10

For this treatment t=500 ms, P=151 watts, d=14.2 mm, so A=0.417 mm^2, and I=1.81x10^4 J/cm^2.

a) The width of the D.Z was 2.25 mm. The D.Z did not vary significantly in size from treatment.8 to treatment.10. A crater with a H.R.P in the center can be observed in Figure.50.

b) No secondary cracking was observed. Primary cracks reached up to 3.4 mm in length.

c) Cleavage steps were very apparent. This is shown by the arrow in Figure.50.

A summary of the laser parameters and the laser damage as indicated by the D.Z width and the length of the cleavage cracks for treatments 8 through 10 is presented in Table.3.

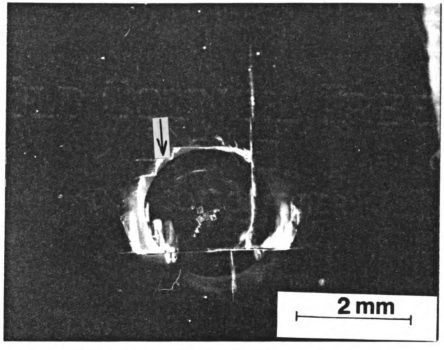

Figure.50 Optical Micrograph Showing the Laser Damage on the Surface and Inside the Bulk for Treatment.10, (Distance from Focus = 14.2 mm and Fluence = 1.80×10^4 Joules/cm^2).

Table.3: Summary of the Results Obtained for Increasing the Distance from Focus from Treatment.8 to Treatment.10

	Treatment.8	Treatment.9	Treatment.10
Pulse Length (ms)	500	500	500
Power (watts)	151	151	151
Distance From Focus (mm)	6.86	8.90	14.22
Energy Density (10^4 Joules/cm^2)	2.74	2.36	1.80
D.Z Width (mm)	2.12	2.20	2.28
Length of The Longest Secondary Cleavage Crack (mm)	3.00	2.27	0.00
Length of The Longest Primary Cleavage Crack (mm)	5.20	4.20	3.65

Important Observations Related to Experiment Sets A, B, and C.

In Figure.51, the scanning electron micrograph of the area between the H.R.P and the edge of the D.Z is prescribed. This area contained bubbled material and was subdivided by what seemed like grain boundaries. This suggested that the melted material had transfomed into a polycrystal during the crystallization that followed the rapid quenching of the molten surface.

The bulk damage due to treatment.8 on the (100) side face of the single crystal after the sample was cleaved through the middle of the D.Z can be seen in Figure.52. This Figure provides the three dimensional shape of the D.Z, which is close to half a sphere with maximum radius equal to 1.1 mm (half the width of the D.Z) and minimum radius equal to 0.7 mm (depth of the D.Z). The interface between the D.Z and the rest of the bulk is very clear. Some material removal can be observed at the interface. The material removal can be due to the effect of compressive forces exerted by the material in the D.Z during the laser pulse. The discontinuity at the interface can suggest a loss of crystallographic coherency between the D.Z and the rest of the bulk. The formation of the D.Z and its separation from the bulk in some areas can be due to 45^{o} (110) slip.

The shape of the D.Z on the surface as described by Figures 27 and 40, can be justified by observing Figure.52.

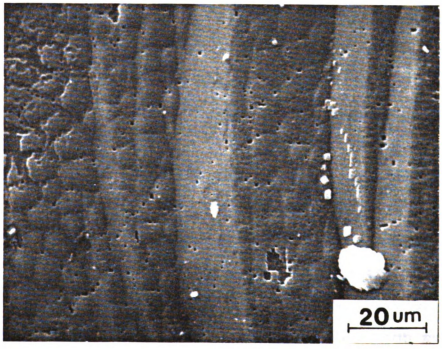

Figure.51 S.E.M Micrograph Showing the Area at the Boundary of the Helix Ripple Pattern for Treatment.10.

A shallow depression (crater) around the center of the D.Z can be observed. Surrounding the crater, some material overflow (although minor for treatment.8) can also be observed. This is indicated by the arrow in Figure.52.

Figure.53 includes three curves of the laser energy density versus the D.Z width for experiment sets A, B, and C. It can be observed that the relationship between the energy density (I) and the D.Z width was almost linear for the range of coordinate values chosen and for all sets of experiments A, B, and C. However, the slope differed from one curve to the other. The high positive slope for the curve (P.L.V), where the pulse length was the variable, indicated the great dependence of the D.Z width on the pulse length as compared to its dependence on the power as shown by the curve P.V where the power was the variable. The slope of curve D.F.V, where the distance from focus was the variable, was low and negative indicating that the width of the D.Z increased as the distance from the focal plane of the laser was increased and therefore the energy density was decreased. The effect of the constant, high pulse length used in set (C) of experiments, overrode the effect of changing the distance from focus on the width of H.A.Z and therefore caused the slope of curve D.F.V to be very low.

Figure.54 is a schematic showing the different laser-induced damage regions on the (001) faces of the LiF single crystals. The damage consists of (1) slip or plastic

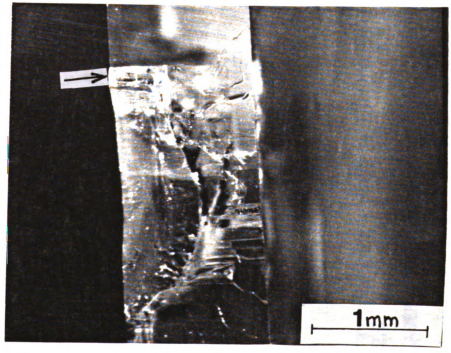

Figure.52 Optical Micrograph Showing the Bulk Damage for Treatment.8 as Observed on the (100) Plane. (Specimen Cleaved to Reveal the Cross-section of the D.Z).

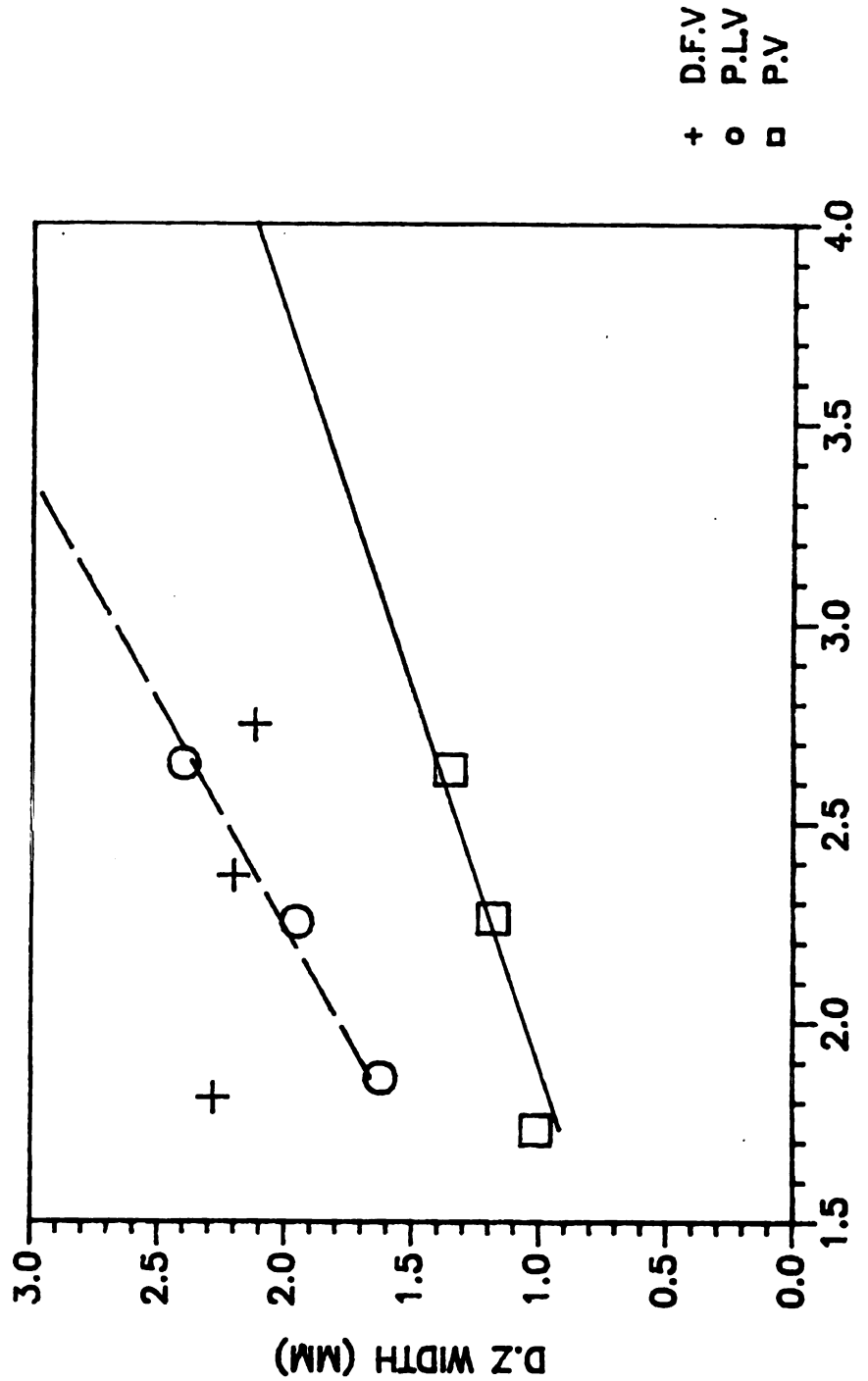

Figure.53 Plot of Laser Energy Density vs. D.Z Width.
D.F.V = Distance from Focus is the Variable,
P.L.V = Pulse Length is the Variable, and
P.V = Power is the Variable.

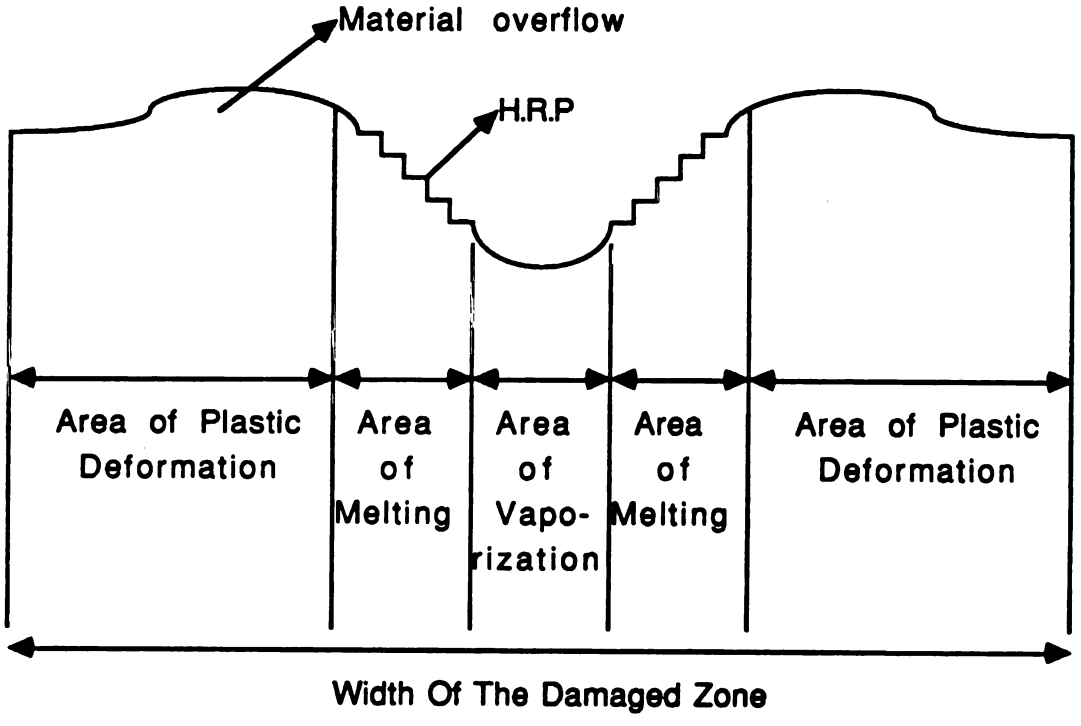

Figure.54 Schematic Showing the Different Damage Regions in Laser Irradiated LiF Single Crystals.

deformation occurring near the edges of the D.Z, (2) melting occurring in an area closer to the center of the D.Z, and (3) vaporization taking place in a relatively small area around the center of the D.Z. The heat was being conducted towards the center of the damaged zone.

Analysis Of The Helix Ripple Pattern (H.R.P).

The helix ripple patterns were observed in treatments that produced shallow craters. This occured when the laser pulse length was high, the beam was focused above the surface or at very low energy densities.

The ripples followed the shape of a helix that started on the surface and worked its way towards the interior of the the bulk. This feature can be observed in the S.E.M micrographs of Figures 55 through 65. The H.R.P in all treatments covered an area smaller than the beam area on the surface. However, its area increased as the beam area increased in set (C) of experiments.

The reason for this particular ripple pattern in the center of the crater area may be due to molten material churning. Turbulence in the molten material may have caused it to recrystallize in the shape of the H.R.P. The H.R.P consists of ripples, in the shape of steps, that descend towards the interior of the bulk. One face of these steps is a (001) plane. This is indicated by the letter (Z) in Figure.58. The other face of the step or ripple, as may be

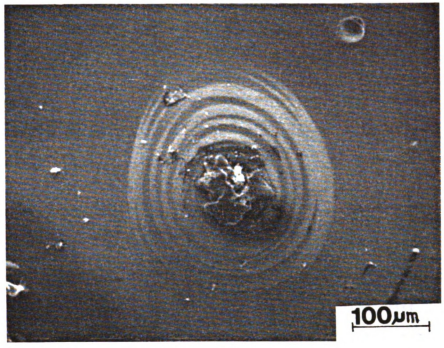

Figure.55 S.E.M Micrograph Showing the H.R.P for Treatment.3.

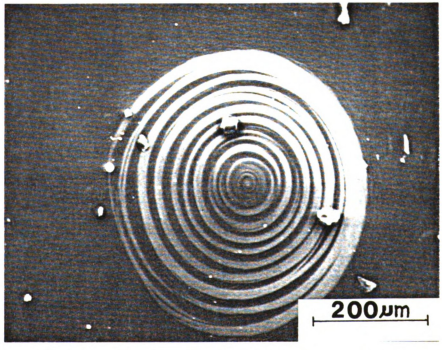

Figure.56 S.E.M Micrograph Showing the H.R.P for Treatment.7.

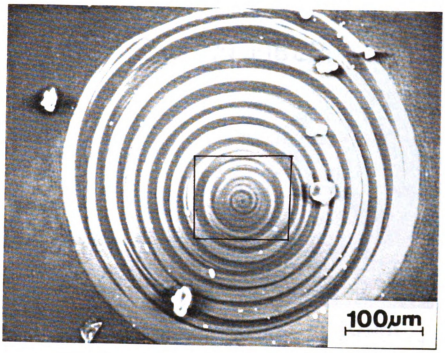

Figure.57 Magnified View of the H.R.P in Figure.56.

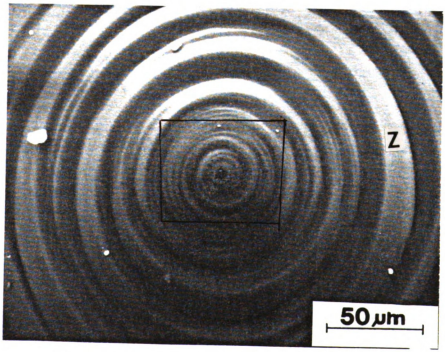

Figure.58 Magnified View of the Area Inside the Square in Figure.57.

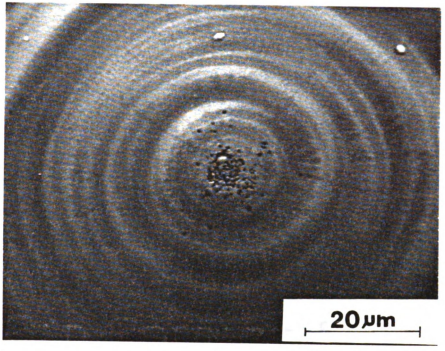

Figure.59 Magnified View of the Region Described by the Square in Figure.58.

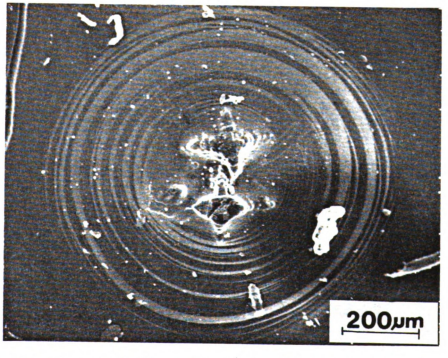

Figure.60 S.E.M Micrograph Showing the H.R.P for Treatment.9.

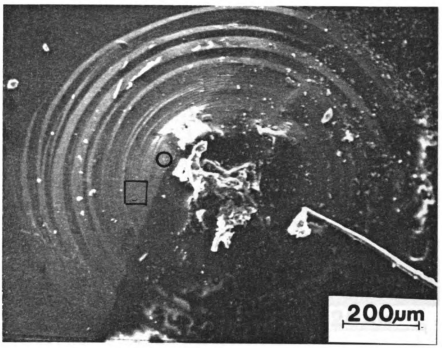

Figure.61 S.E.M Micrograph Showing the H.R.P for Treatment.10.

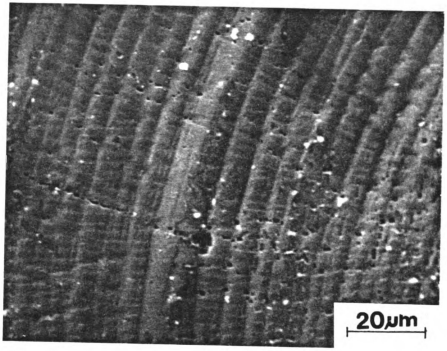

Figure.62 Magnified View of the Area Inside the Square in Figure.61.

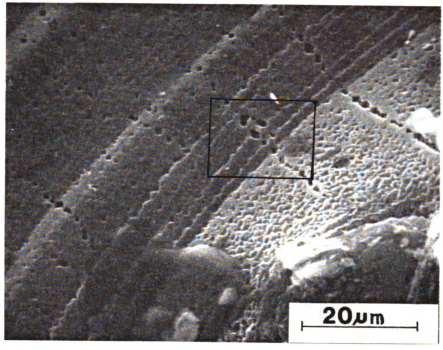

Figure.63 Magnified View of the Area Inside the Circle in Figure.61.

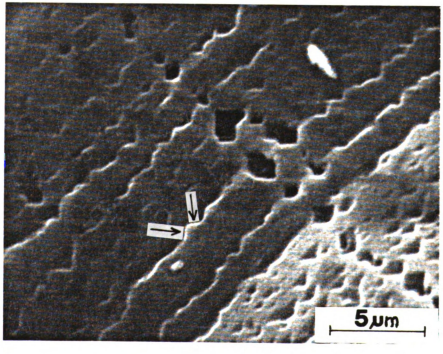

Figure.64 Magnified View of the Area Inside the Square in Figure.63.

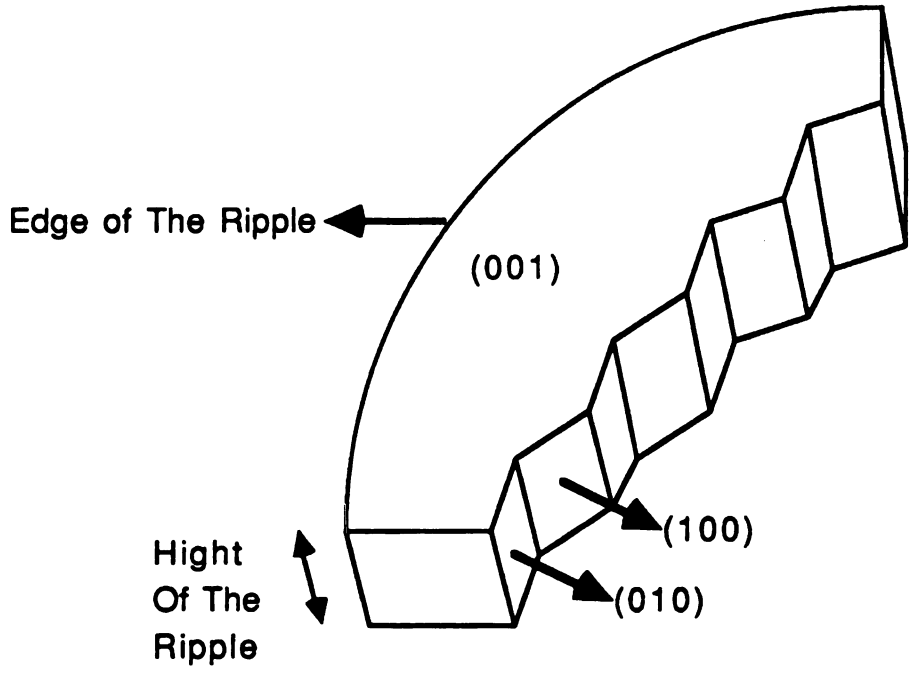

Figure.65 Schematic Showing the Cross-section View of a Ripple in the H.R.P for Treatment.10 as Shown in Figure.64.

analyzed by observing Figures 63 and 64, appear to be bounded by alternating (100) and (010) planes as is indicated by the ridges on the (001) faces of the ripples. The ridges are indicated by the arrows in Figure.64. This can also be observed in the shematic shown in Figure.65. The {100} planes are energetically more favorable for formation in recrystallized LiF as compared to {110} planes based on surface energy considerations. This reinforces the above speculations related to the shape of the ripple.

The formation of the H.R.P may also be due to internal reflection effects of the laser beam.

Further studies will be needed to verify the above speculations or to find the actual mechanisms responsible for the formation of the H.R.P.

D. Slip Due to Laser Heating.

In this part of the study, two samples used were etched for 10 to 15 seconds in a very dilute solution of ferric chloride in water.

The slip lines revealed by etching were of two types. Thick slip lines that could be seen at low magnifications (20X to 40X) and thin slip lines that were seen at higher magnifications, above 50X.

The thick slip lines looked like rays that emanated from the edge of an area surrounding the D.Z where slip lines were not observed. This can be seen in Figures 66 through

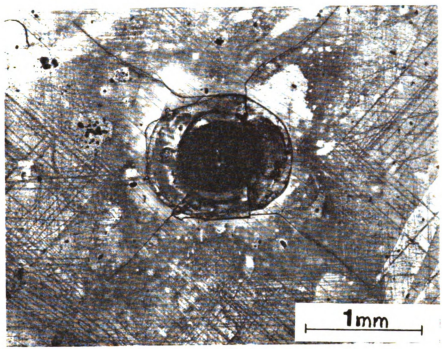

Figure.66 Optical Micrograph Showing the Dislocation Etch Pit Pattern Outside the D.Z for Treatment.1.

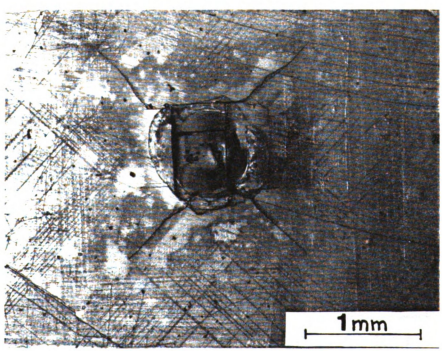

Figure.67 Optical Micrograph Showing the Dislocation Etch Pit Pattern Outside the D.Z for Treatment.2.

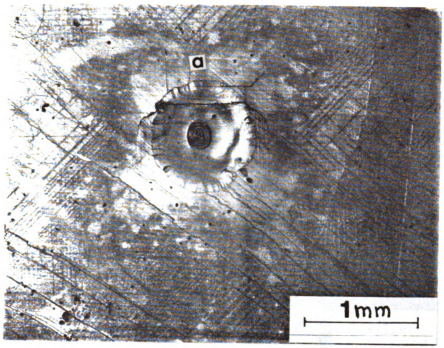

Figure.68 Optical Micrograph Showing the Dislocation Etch Pit Pattern Outside the D.Z for Treatment.3.

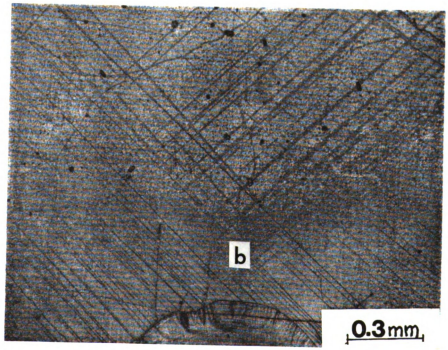

Figure.69 Optical Micrograph Showing a Magnified View of the Area Marked by (a) in Figure.68.

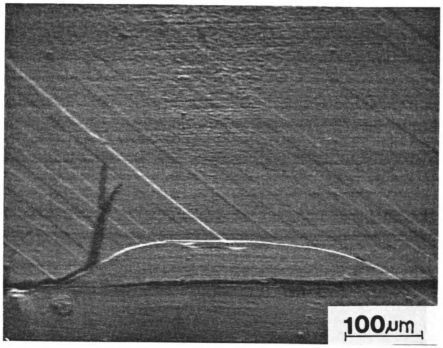

Figure.70 Optical Micrograph Showing a Magnified View of the Area Marked by (b) in Figure.69.

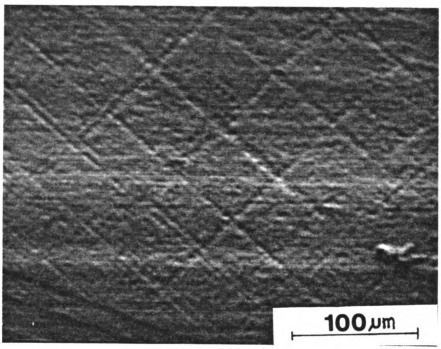

Figure.71 S.E.M Micrograph Showing 90^{o} (110) Slip Lines Just Outside the D.Z for Treatment.2. (Region Above the D.Z in Figure.70).

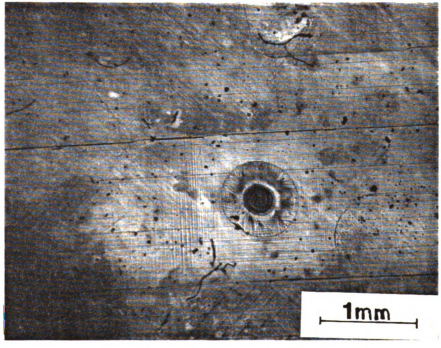

Figure.72 Optical Micrograph Showing the Dislocation Etch Pit Pattern Outside the D.Z for Treatment.7.

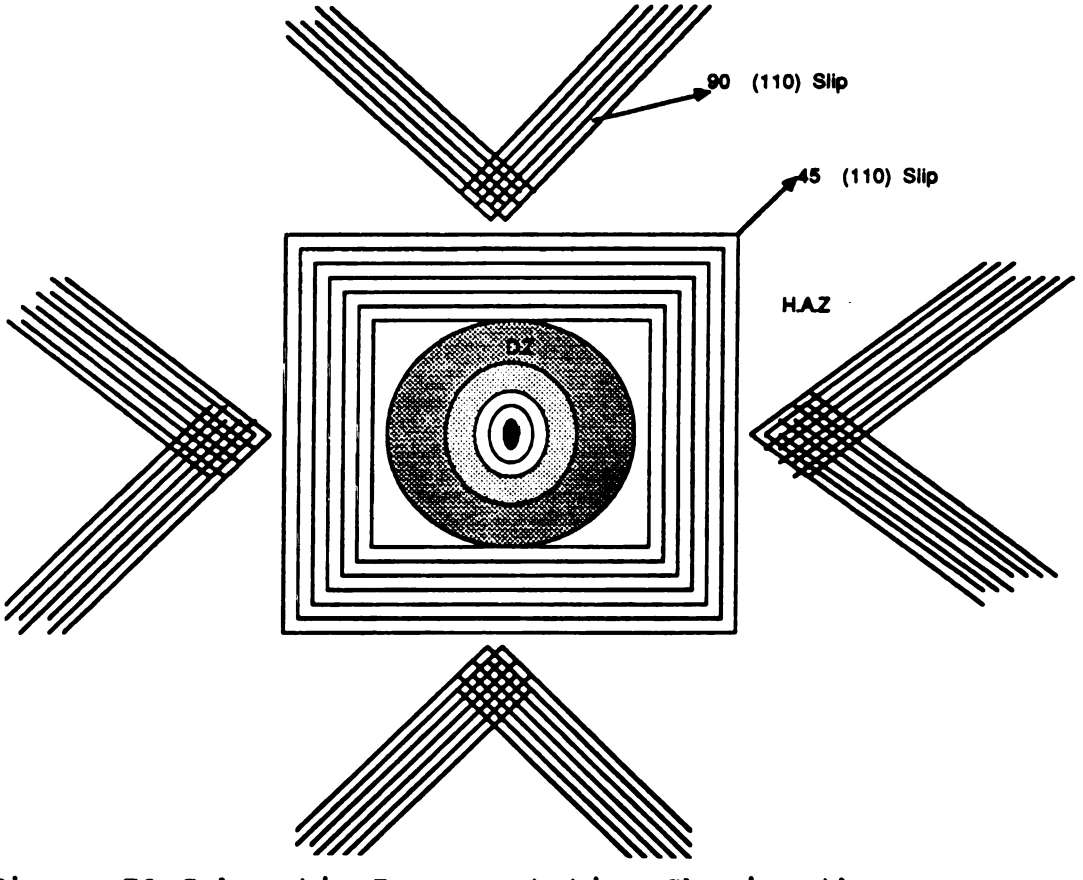

Figure.73 Schematic Representation Showing the Dislocation Etch Pit Pattern Outside the D.Z for Treatment.7.

71. However, the micrograph of Figure.72 indicated that 45° primary slip was present in the area immediately surrounding the D.Z. This type of primary slip is usually hard to observe due to shallow dislocation etch pits on the surface or due to the interference between the 90° (110) slip lines and the 45° (110) slip lines. The 45° slip surrounding the D.Z could be responsible for the formation of the smooth, curved shape of the D.Z inside the bulk as was seen in Figure.54. Figure.73 is a schematic representation of the slip lines observed in the micrograph of Figure.72. The thick slip lines followed primary <110> slip directions on the (001) surface of the LiF single crystals. The dislocation motion inducing slip can be due to mechanical stress fields produced by the laser irradiation.

Tensile stresses caused by the rapid quenching of the surface, were created when the laser pulse was completed. These stresses were thought to be responsible for controlling the slip distribution outside the D.Z [20]. According to Gorbunov et.al [20], the compressive stresses due to the temperature gradient imposed on the surface during the laser heating phase had the same magnitude as the tensile stresses, however they didn't last long enough to control the slip distibution outside the damaged zone in copper single crystals.

To explain the effect of thermal stresses on the motion of dislocations and their specific slip planes, we can use

the same approach Haessner [22] used for copper single crystals. He suggested a quantitative analysis to assess the necessary forces acting on dislocations which cause slip. He assumed

$$\vec{K}=[\vec{F} \times \hat{n}] \times \hat{n} \qquad (9)$$

was the component of the force

$$\vec{F}=\underset{\sim}{\sigma}.\vec{b} \times \vec{L} \qquad (10)$$

which acted on a dislocation with burgers vector $\vec{b}$ and dislocation line $\vec{L}$ in its slip plane (unit vector $\hat{n}$) when an external stress field (tensor $\underset{\sim}{\sigma}$) was applied.

The thermo-mechanical stress field $\underset{\sim}{\sigma}$ produced by laser irradiation was derived by Bailey[22]. Bailey suggested a stress field with radial symmetry (as shown in Figure.74) if the Young's modulus (E) and the linear expansion coefficient (β) are isotropic. The stress field on the surface (z=0) is defined by:

$$\sigma_{rr}=-(1/2)E\beta(\delta T)(R/r)^2 \qquad \text{for } r>R, \qquad (11)$$

$$\sigma_{\phi\phi}=+(1/2)E\beta(\delta T)(R/r)^2 \qquad \text{for } r>R, \text{ and} \qquad (12)$$

$$\sigma_{rz}=\sigma_{zz}=0 \qquad (13)$$

where (R) is the D.Z radius and (δT) is the temperature increase on the surface due to the laser heating [22].

Equations (11),(12) and (13) could be used to calculate the force (K) as a function of (r) and (ϕ) for the case of LiF single crystals, laser shocked on (001) faces. The values of (ϕ) for which slip occurred were ϕ= 45°, -45°, 135°, and -135°. K should assume its maximum values at

these values of (ϕ).

Thin slip lines originating inside the D.Z can be easily observed, particularly for treatments with low energy densities like treatments 3,5, and 9. These slip lines can be observed at magnifications above 50X as can be seen in Figures 75 through 80. The S.E.M micrograph of Figure.81, however, indicated the existence of slip lines inside the D.Z for treatment.1 which had the highest energy density.

Slip lines in Figures 80,24, and 25 of treatment.3 formed a parallelogram around the rippled area inside the D.Z. The slip line structure in this case could be controlled by the compressive stresses as opposed to the tensile stresses acting outside the H.A.Z. Figure.82 is a schematic representing the slip line configuration inside the D.Z for treatment.3 with low energy density.

Figures 78, 83, and 84 indicate (110) slip lines that intersect at a (001) crack. Slip in this case was induced by the crack propagation, as opposed to those in indentation experiments, where the (001) cracking was induced by the pile up of dislocations on intersecting {110} planes [29].

Crack propagation can induce the nucleation of dislocations in LiF when the crack velocity is less than $6x10^3$ cm/sec [35]. At velocities less than $3x10^3$ cm/sec, the crack velocity in a lithium fluoride crystal oscillates between a high and a low value as compared to a critical velocity. As the crack slows down, dislocations are formed.

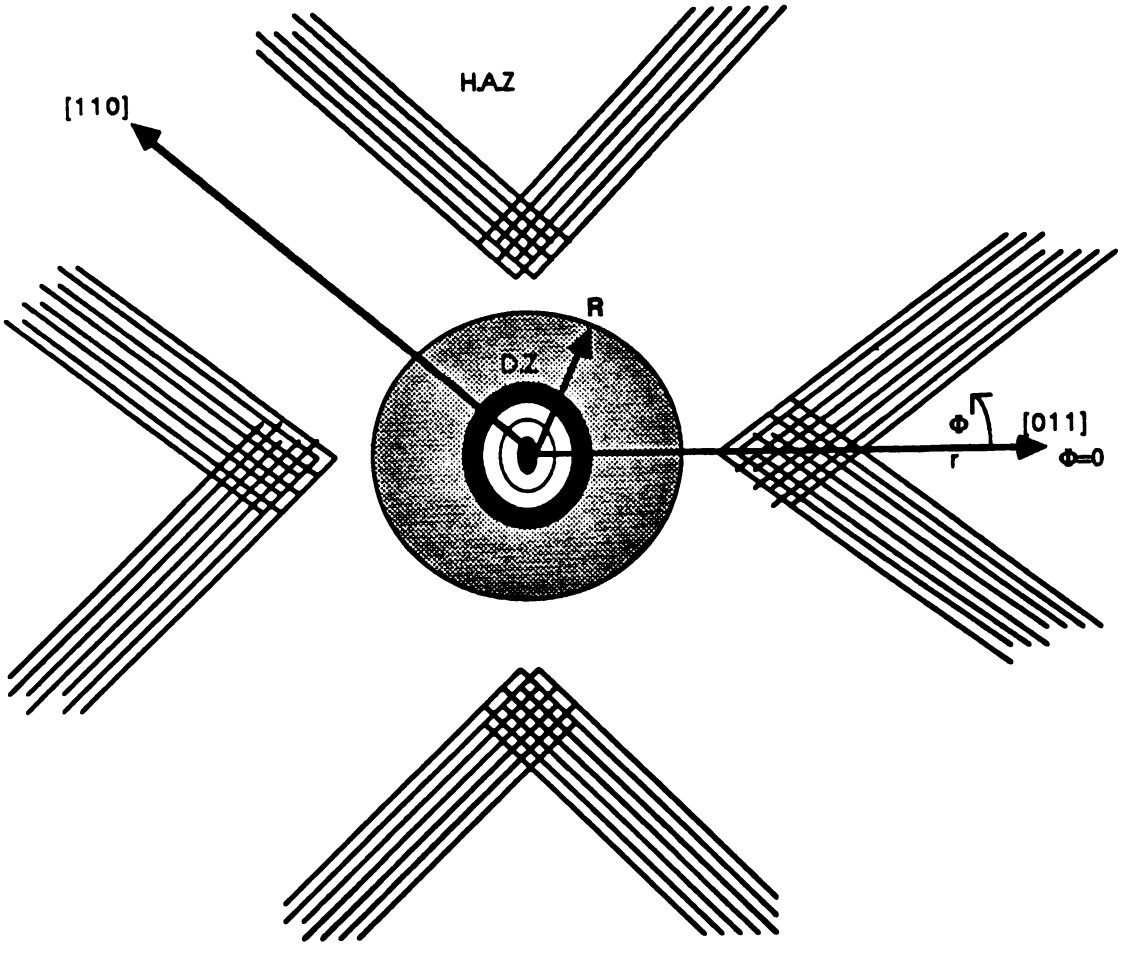

Figure.74 Cylindrical Coordinate System for the Thermal Stress Field Outside the Laser Induced D.Z on the (001) Face of LiF Single Crystals.

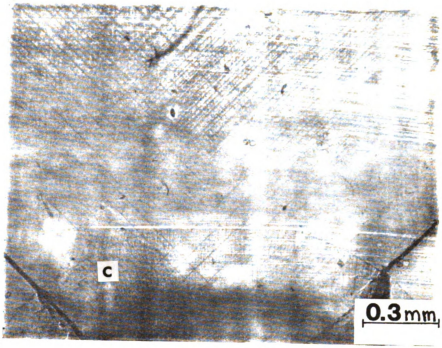

Figure.75 Optical Micrograph Showing the Dislocation Etch Pit Pattern Inside the D.Z for Treatment.9. (Top Half of the D.Z in Figure.47).

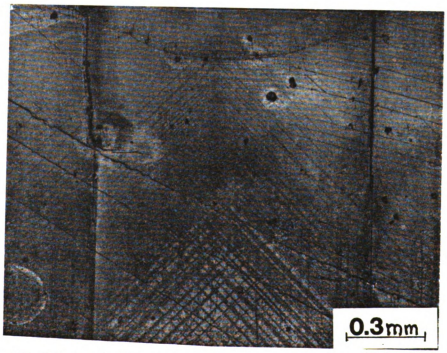

Figure.76 Optical Micrograph Showing the Dislocation Etch Pit Pattern Inside the D.Z for Treatment.9. (Bottom Half of the D.Z in Figure.47).

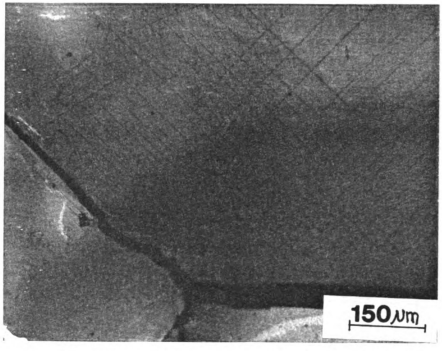

Figure.77 Optical Micrograph Showing a Magnified View of the Area Marked by (c) in Figure.75.

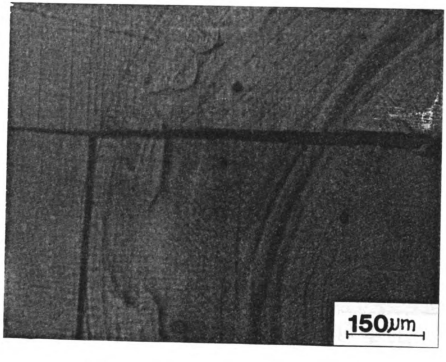

Figure.78 Optical Micrograph Showing the Slip Lines in Regions Adjacent to a Crack Inside the D.Z for Treatment.5.

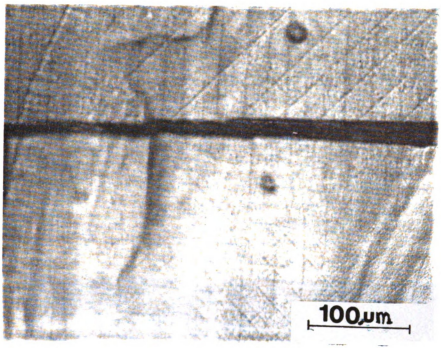

Figure.79 Optical Micrograph Showing a Magnified View of the Slip Lines Adjacent to the Crack in Figure.78.

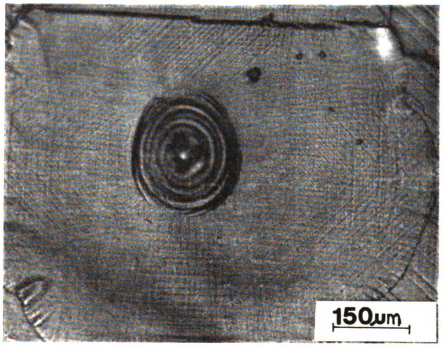

Figure.80 Optical Micrograph Showing the Dislocation Etch Pit Pattern Inside the D.Z for Treatment.3.

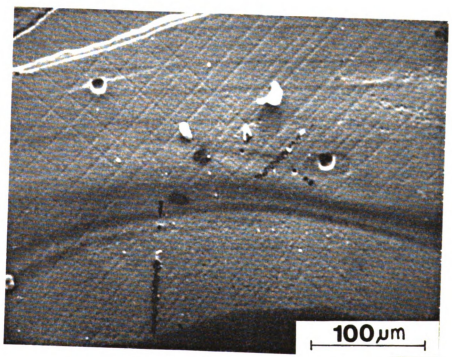

Figure.81 S.E.M Micrograph Showing Slip Lines in the Area Between the Crater and the Edge of the D.Z for Treatment.1.

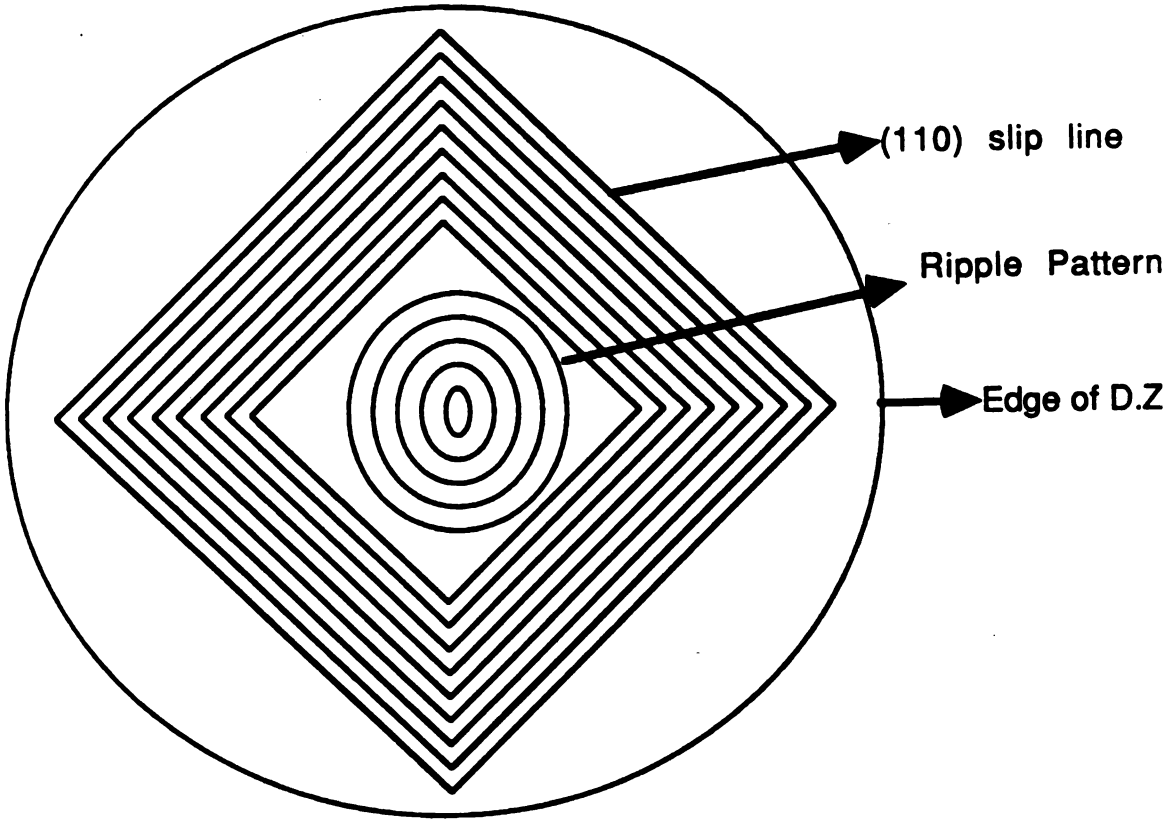

Figure.82 Schematic Representation of the Slip Line Distribution as Observed Inside the D.Z for Treatment.3

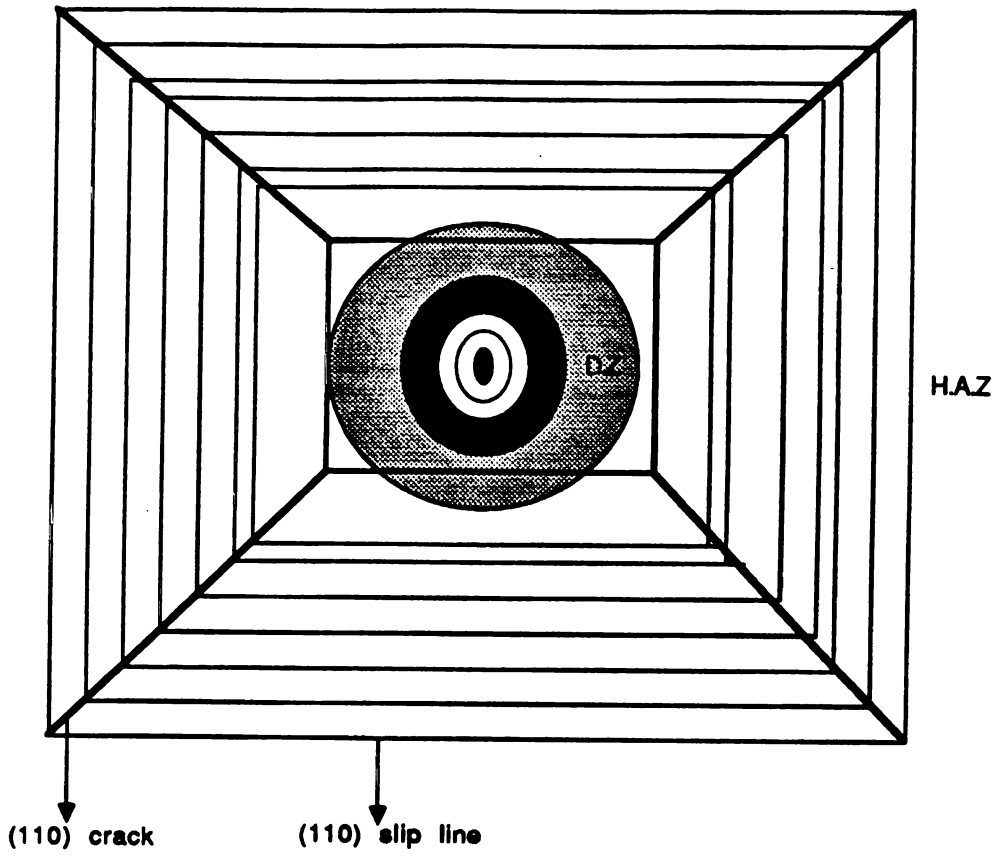

Figure.83 Schematic Representation of Slip Lines Induced by (110) Cracks on the (001) Surface of LiF Single Crystals.

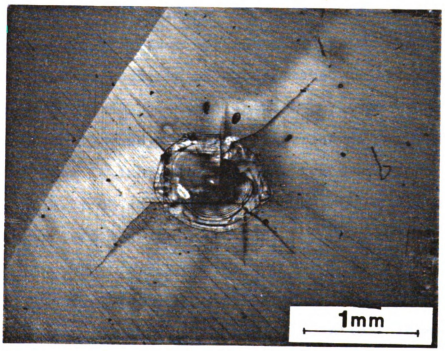

Figure.84 Optical Micrograph Showing Slip Lines induced by (110) Cracks.

This absorbs energy which slows it down further. The crack should soon stop propagating unless more force is applied to the crystal. However, the cleaved ends of the crystal are moving apart at constant velocity which builds up force to drive the crack forward after it has slowed down. When this force is high enough, the crack begins to accelerate again. As the crack accelerates, fewer dislocations are formed requiring less force to move it, and it continues to acceelerate. The crack would accelerate up to the terminal velocity if the driving force did not decrease when the crack is moving fast again compared with the rate at which the cleaved ends are being seperated. The crack, therefore slows down and the cycle is then repeated [35].

According to Mott[35], the crack velocity is lowest when the crack is longest. The slip traces induced by cracks , especially at regions close to the end or tip of the cracks can be seen in Figure.86.

E. Effect of Sample Thickness on Laser Damage Propagation

Three laser treatments with identical laser variables (power, pulse length and distance from the focal plane) were carried out on the (001) planes of three LiF single crystals with different thicknesses. The crack lengths and the width of the D.Z were recorded. This was to reveal the effect of the sample thickness on the extent of laser damage.

The laser variables were kept constant at t=340 ms,

P=207 watts, d=0 mm, so A=0.245 mm^2 and I=2.87x10^4 J/cm^2.

1) Treatment.11

For this treatment, the sample thickness was th=3.8 mm, and the sample width was w=14.5 mm.

The D.Z width was 0.9 mm and the length of secondary cleavage cracks reached a length of 0.7 mm. This was measured from Figure.85.

2) Treatment.12

For this treatment, the sample thickness was th=2.8 mm, and the sample width was 14.5 mm.

The D.Z width was 0.97 mm and the secondary cracks reached 0.87 mm in length. This was calculated from figure.86.

3) Treatment.13

For this treatment, The sample thickness was th=1.6 mm and the the sample width was 14.5mm.

The D.Z width was 1.4mm.

In this treatment.13, primary cracking was prevalent as shown in Figure.87. The primary cracks reached a maximum length of 1.84 mm in length.

Table.4 is a summary of all the results found in this set of experiments.

The results of Table.4 indicated an obvious relationship

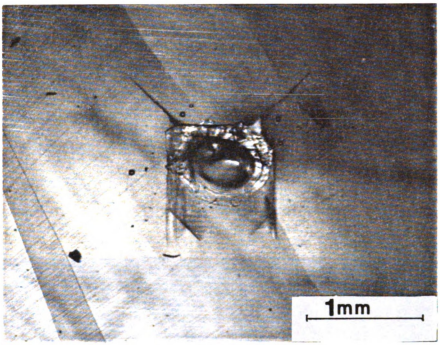

Figure.85 Optical Micrograph Showing the Laser Damage for Treatment.11, (Sample Thickness = 3.8 mm and Fluence = 2.87×10^4 Joules/cm^2).

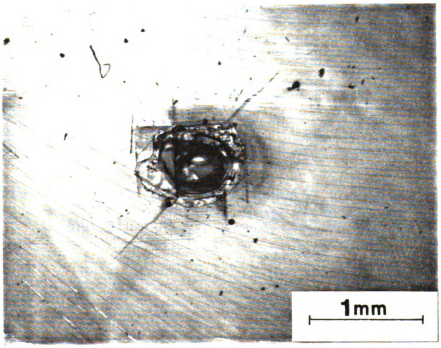

Figure.86 Optical Micrograph Showing the Laser Damage for Treatment.12, (Sample Thickness = 2.8 mm and Fluence = 2.87×10^4 Joules/cm^2).

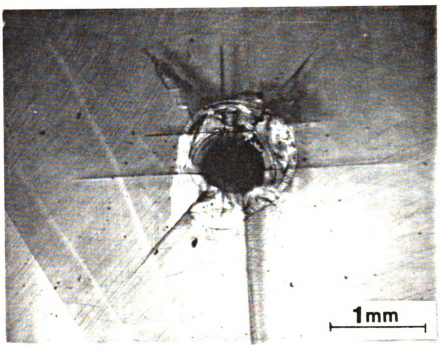

Figure.87 Optical Micrograph Showing the Laser Damage for Treatment.13, (Sample Thickness = 1.6 mm and Fluence = 2.87×10^4 Joules/cm^2).

Table.4: Laser Damage Dependency on Sample Thickness.

	Treatment.11	Treatment.12	Treatment.13
Sample Thickness (mm)	3.8	2.8	1.6
Pulse Length (ms)	340	340	340
Power (watts)	207	207	207
Distance From Focus (mm)	0.00	0.00	0.00
Energy Density (10^4 Joules/cm^2)	2.87	2.87	2.87
D.Z Width (mm)	0.90	0.97	1.40
Length of The Longest Secondary Cleavage Crack (mm)	0.67	0.87	1.08
Length of The Longest Primary Cleavage Crack (mm)	0.90	0.90	1.84

between the sample thickness and the amount of laser damage described by the length of the cracks and the D.Z width. Both the crack length and the D.Z width increased with decreasing sample thickness. However the relationship described is non-linear as both values of The D.Z width and the length of cracks increased drastically from thickness th=2.8 mm to th=1.6 mm. This could be observed in the graphs provided in Figures 88 and 90. Comparison of the graphs given in Figures 88 and 89 indicates that the variation of the length of secondary cleavage cracks with the sample thickness is more linear than that for the primary cleavage cracks. It was also observed that primary cracking predominated at small values of the sample thickness.

Experimental observations indicated that samples with small thicknesses may have allowed higher absorption of the laser radiation than thicker samples. Crack propagation in thin samples may have been made easier by less obstacles in the crack path as compared to thicker samples. As a result, there is less constraint for primary cleavage to propagate. This is probably the reason for the predomination of the primary cleavage cracking during laser irradiation of thin samples. Also, for thin enough samples, the laser light could be reflected after reaching the metallic support. The reflected energy is then absorbed by the sample and causes an increase in the amount of laser-induced damage.

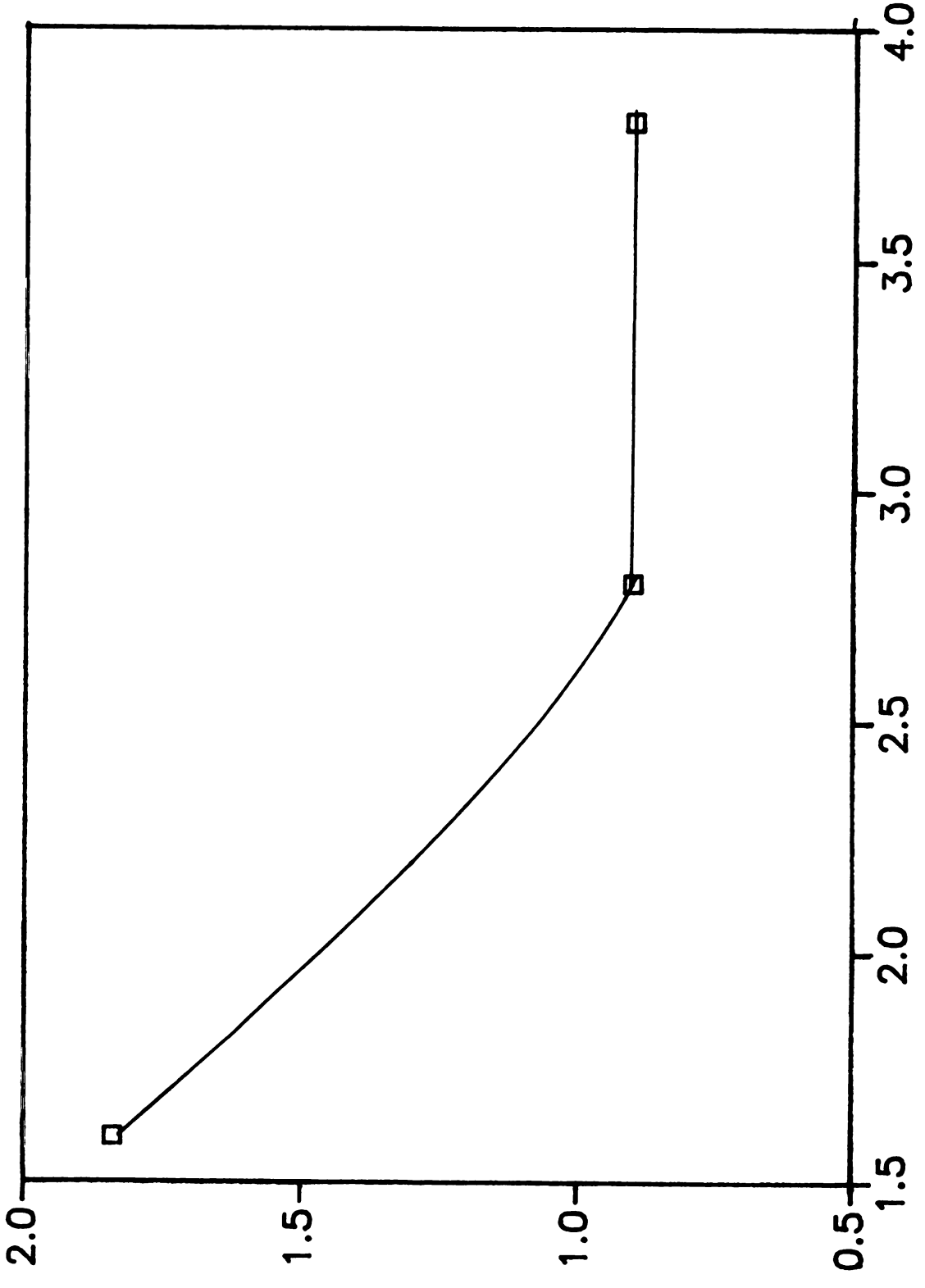

Figure.88 Plot of Sample Thickness vs. Maximum Primary Cleavage Crack Length.

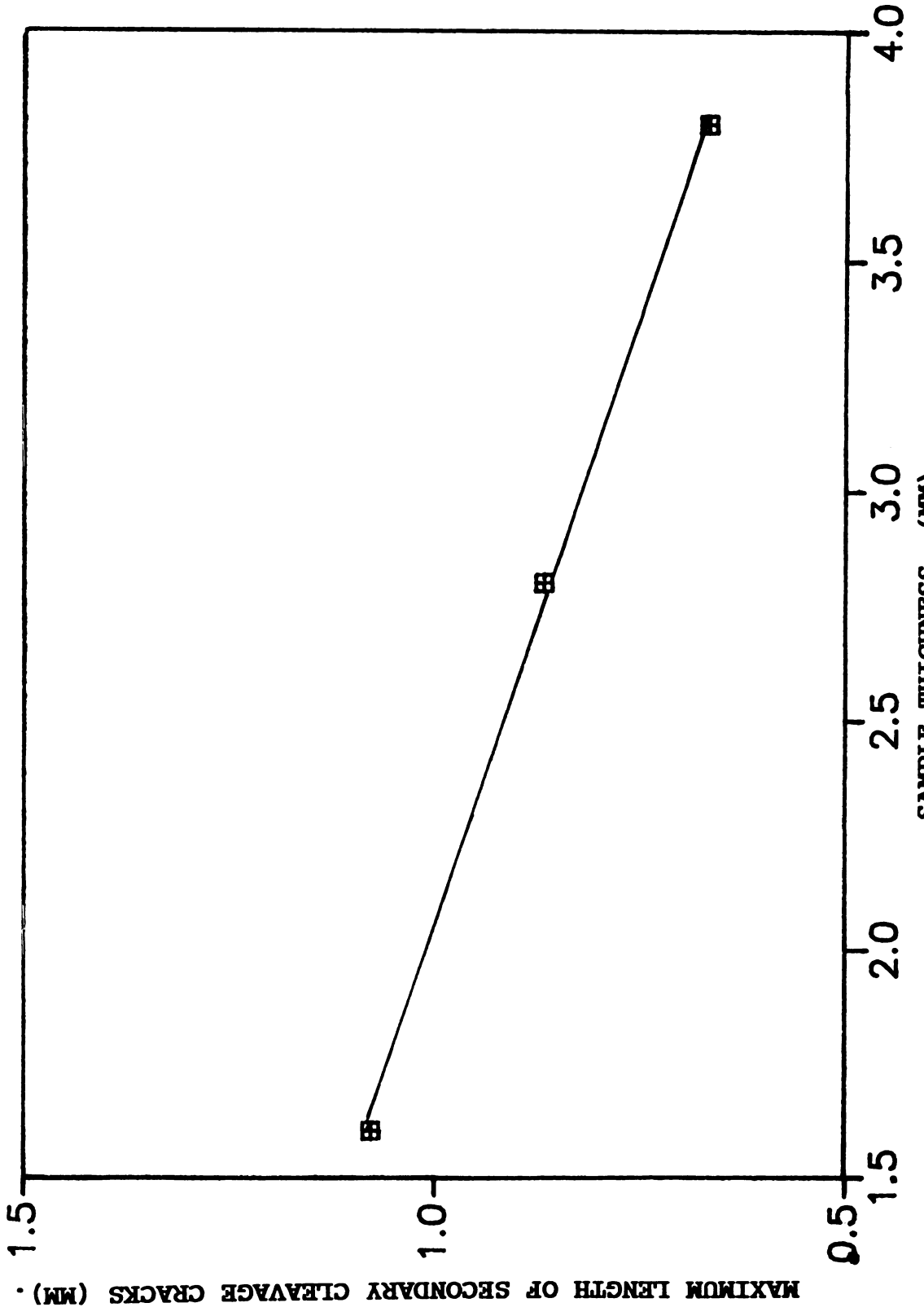

Figure.89 Plot of Sample Thickness vs. Maximum Secondary Cleavage Crack Length.

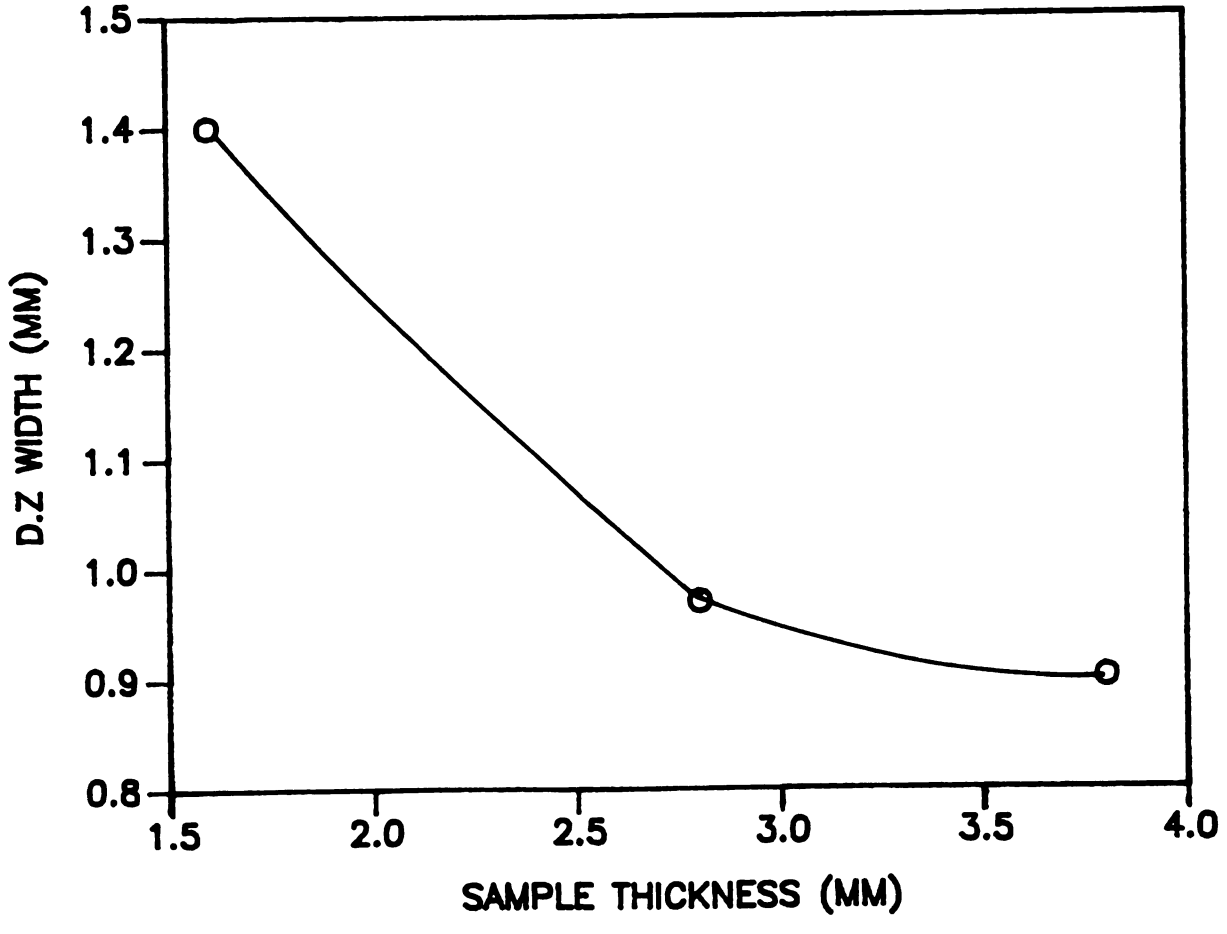

Figure.90 Plot of Sample Thickness vs. D.Z Width.

V. CONCLUSIONS:

1. A heat Damaged zone (D.Z) is observed for all laser treatments shown. This is an area where evaporation, melting, and plastic deformation as indicated by slip can occur. The mechanism of formation of this zone may be due to the 45° (110) primary slip. The extent of each form of damage depends on the extent of the laser variables and the energy density. The dimensions of the D.Z and its characteristics change as the laser energy density changes. Rippling of the surface around the crater (area usually just larger than the beam area) is seen even at very low energy densities. Rippling is an indication of the plastic deformation that occurs during laser heating.

2. A ripple pattern in the shape of a helix is observed around the area of evaporation in the center of the D.Z for treatments that produced shallow craters. This occurs when the laser pulse length is large, the laser beam is focused above the surface, or at very low energy densities.

3. Primary (100) and secondary (110) cleavages due to laser irradiation are observed on the (001) face of the LiF single crystals.

4. Non-crystallographic cracks are only abundant for treatments with low values of the pulse length.

5. The pulse length has the most critical influence on the extent of damage. A small change in the pulse length can induce a significant change in the amount of laser damage as

indicated by the changes in the D.Z width and the length of secondary cracks. Increasing the pulse length increases the time of laser interaction with the surface, causing the damage to propagate over larger areas.

6. Increasing the laser power, however, mainly increases the depth of the crater and induces more material overflow on the D.Z. Also, the cracks are longer and the D.Z is wider but these two featues are much more sensitive to the pulse length.

7. An increase in the distance from the focal plane of the laser to the specimen surface, mainly decreases the length of the primary and the secondary cracks. Primary cleavage cracks become the prevalent sort of cleavage as the distance from focus is increased. The width of the D.Z seems to increase very slowly as the energy density is decreased for the case where the constant pulse length is large. It is suggested that repeating the treatments with changing distance from the focus for a lower value of the pulse length can result in larger differences in the width of the D.Z as the energy density is decreased. In this case the dominating effect of the pulse length would be reduced.

8. Slip is observed inside the D.Z as well as outside (H.A.Z). The slip distribution observed inside the D.Z is different from that observed outside. Compressive stresses due to the temperature gradient during the laser pulse are thought to control the slip distribution inside the D.Z,

while the thermal tensile stresses due to the quenching effect on the surface control the slip distribution outside.

9. The fluctuations in the crack velocities result in variations in the dislocation density as the crack propagates.

10. Propagation of cracks results in slip.

11. The sample thickness, below a certain value, affects the extent of damage due to the laser-treatment. The D.Z width and crack length augment as the sample thickness decreases. This could be due to absorption of laser energy reflected from the metallic support underneath the sample.

12. Because of the transparency of LiF, optical microscopy was shown to reveal more of the laser damage as compared to scanning electron microscopy. However, scanning electron microscopy can be more advantageous in revealing the surface damage.

VI. RECOMMENDATIONS

1) Transmission electron microscopy ought to be used in order to reveal the origins of the damaged zone and the reasons for its very well defined circular shape.

2) A thick sample should be used for the experiments with the laser focal point being away from the sample surface. This will eliminate the effect of thin samples on the propagation of damage.

3) Further studies are needed to clarify the mechanism of formation of the helix ripple pattern. High resolution electron microscopy might be very useful for clarifying this mechanism.

4) Further studies may also be necessary to clarify the reasons for the effect of the sample thickness on the extent of the laser-induced damage. A thick sample where one treatment has been carried out, can be cleaved to reduce its thickness; then one more treatment having the same laser variables as the previous can be carried out on a spot which location is close to that of the previous treatment. This is to eliminate the effects of the surface roughness on the absorption of the laser radiation. Also, two very thin samples can be superimposed before carrying out the laser treatment in order to check for laser-induced damage on the surface of the bottom sample. This can help identify and verify the effect of the sample thickness on the propagation of damage.

APPENDIX A

Some Thermal Properties of LiF Single Crystals

Melting Point = 845°C [36]

Boiling Point = 1676°C [36]

Enthalpy of Fusion = 91.1 cal/gram [36]

Heat Capacity at 25°C, C_p = 9.994 cal/mol deg [37]

APPENDIX B

Infrared Absorption Edges of Ionic Crystals

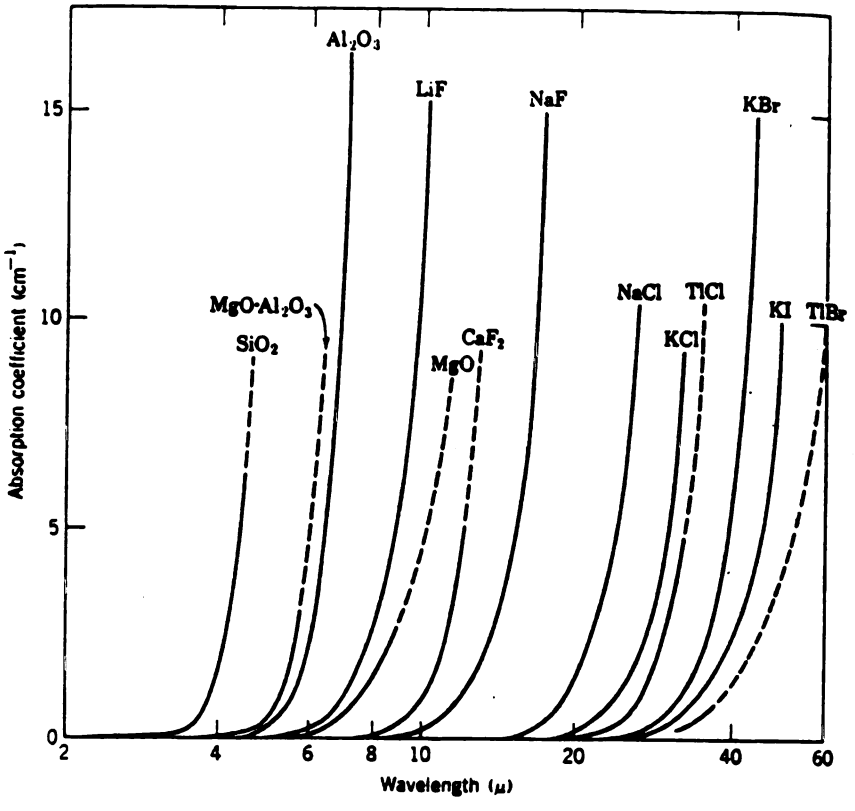

Figure.91 Plot of Absorption Coefficient vs. radiation wavelength. (From [11]).

REFERENCES

1. McGraw-Hill Encyclopidia of science and technology 7, p. 547, 5th edition, Vol 7, McGraw-Hill, Inc., New York, 1982.

2. A. Lytel and L. Buckmaster, ABC's of Lasers and Masers, p. 13, Howard W. Sams & Co., Inc., 1972.

3. Dieter Ross, Lasers: Light Amplifiers and Oscillators, p. 456-459, edited by O. S. Heavens, Academic Press, New York, 1969.

4. F. A. Jenkins, Fundamentals of Optics , p. 447-468, third edition, McGraw-Hill, Inc., 1957.

5. P. R. Clayton and S. A. Nasar, Introduction to Eletromagnetic Fields, p. 301, McGraw-Hill, Inc., 1987.

6. E. Wolf, Principles of Optics, p.3, 5th edition, Pergamon Press, 1975.

7. R. Berman, Thermal Conduction in Solids, p.6, Clarendon Press, Oxford, 1976.

8. Max Born and Emil Wolf, Principles of Optics, p.608, second edition, Pergammon Press, 1959.

9. J. M. Bennet and J. M. Elson, Laser Induced Damage in Optical Materials: 1977, p. 142, An NBC Special Publication 509, ASTM STP 655, 1977.

10. N. M. Tallan, Electical Conductivity in Ceramics and Glass (part A), p.13, Marcel Dekker, Inc., 1974.

11. W. D. Kingery, H. K. Bowen, D. R. Uhlmann, Introduction to Ceramics, p. 583-586,604, and 373, 2nd edition, J. Wiley & Sons, Inc., 1976.

12. B. Schultrish, and K. Wetzig, "Investigation of Laser irradiation of WC-Co Cemented Carbides Inside a Scanning Electron Microscope (LASEM)," J. Mater. Sci., 22, 3361, 1987.

13. F. D. Seaman and D. S. Gnanamuthu, "Using the Industrial Laser to Surface Harden and Alloy," Met. Progress., 108, 67, August, 1975.

14. C. W. Drapper, "The Use of Laser Surface Melting to Homogenize Fe-Al Bronzes," J. Mater. Sci., 16, 2774, 1981.

15. K. Mukherjee, N. Dahotre, and C. Wakade, "Shear Band Formation and Cracking of a Metallic Glass Irradiated with High Energy Laser Pulses," J. Mater. Sci., 22, 601, 1987.

16. H. A. Bahr, G. Fisher, H. J. Weiss, "Thermal-Shock Crack Patterns Explained by Single and Multiple Crack Propagation," J. Mater. Sci., 21, 2718, 1986.

17. A. H. Clauer, Third Advanced Material Workshop, Traverse City, Michigan, September 15-17, 1986.

18. L. D. Merkle, M. Bass and R. T. Swimm, Laser Induced Damage in Optical Materials:1982, p. 50-52, An NBC special publication 669, ASTM STP 847, 1982.

19. H. M. Musual, Jr., Laser Induced Damage in Optical Materials:1979, p. 159, An NBS Special Publication 568, ASTM STP 726, 1979.

20. A. V. Gorbunov, E. B. Leiko, E. M. Nadgornyi, and S. N. Valkovskii, "Pecularities of Laser-Induced Dislocation Structure in Mo Single Crsystals," Scripta Metall., 14, 417, 1980.

21. Y. Jee, M. F. Becker, and R. M. Walser, Use of Lasers in Materials Proceesing Applications, p. 575, The Laser Institute of America, Toledo, Ohio, 1987.

22. F. Haessner and W. Seitz, "Laser-Induced Dislocation Structures in Copper Single Crystals," J. Mater. Sci., 6, 16, 1971.

23. J. O. Porteus, C. W. Fountain, and M. J. Soileau, Laser Induced Damage in Optical Materials: 1976, p. 165, An NBC Special Publication 462, ASTM STP 622, 1976.

24. J. O. Porteus, C. W. Fountain, J. L. Jernigan, W. N. Faith, and H. E. Bennet, Laser Induced Damage in Optical Materials: 1977, p.204, An NBC Special Publication 509, ASTM STP 655, 1977.

25. O. T. Inal and L. E. Murr, "Laser-Shock-Induced Microstructural changes and a Comparison with Explosive-Shock-Induced Phenomena in Metals: Field-Ion and Electron Microscopic Studies," J. Appl. Physics, 49, 2427, 1978.

26. J. A. McMordie and P. D. Roberts, "The Interaction of Pulsed CO_2 Laser Radiation with Aluminum," J. Phys. D: Appl. Physics, 8, 779, 1975.

27. J. J. Gilman, "Plastic Anisotropy of LiF and Other Rocksalt-type Crystals," Acta Metall., 7, 608, 1959.

28. M. J. Zawisza, Laser Induced Damage in Lithium Fluoride Single Crystals, B.S Thesis, Michigan State University, East Lasing, Michigan, 1986.

29. J. Y. Lee, Fracture and Deformation of Lithium Fluoride Bicrystals Under Impact Erosion and Quasi-static Indentation, Ph.D Thesis, Michigan State University, East Lansing, Michigan, 1985.

30. K. N. Subramanian, Work Hardening and Deformation Structure In Lithium Fluoride Single Crystals, Ph.D Thesis, Michigan State University, East Lasing, 1966.

31. S. M. Wiederhorn, Mechanical and Thermal Properties of Ceramics, p. 217, An NBS Special Publication 303, 1968.

32. J. Y. Lee, Crack Propagation in Lithium Fluoride Bicrystals, M.S Thesis, Michigan State University, East Lansing, Michigan, 1982.

33. D. H. Hull, and D. J. Bacon, Introduction to Dislocations, p.57, Third Edition, Pergamon Press, 1984.

34. M. M. Chaudhri, J. K. Wells, and A. Stephens, "Dynamic Hardness, Deformation and Fracture of Simple Ionic Crystals at Very High Rates of Strain," Phil. Mag. A , 43, 643, 1981.

35. J. J. Gilman, C. K. Dsen, and W. P. Walsh, "Cleavage Cracks and Dislocations in LiF Crystals" J. Appl. Physics, 29, 601, 1958.

36. Handbook of Chemistry and Physics, 71 st edition, 1990-1991, edited by D. R. Lide, CRC Press Inc., 1990.

37. Comprehensive Inorganic Chemistry, Vol 1, edited by A. F. Trotman-Dickenson, Pergamon Press, 1973.